

1           **STATE-OF-THE-ART INVESTIGATION OF WIND TURBINE**  
2           **STRUCTURES FOUNDED ON SOFT CLAY BY CONSIDERING THE**  
3           **SOIL-FOUNDATION-STRUCTURE INTERACTION PHENOMENON –**  
4           **OPTIMIZATION OF BATTERED RC PILES**

5                           **Dewald Z. Gravett<sup>1\*</sup> and George Markou<sup>1†</sup>**

6                           <sup>1</sup>Department of Civil Engineering, University of Pretoria, South Africa  
7                           e-mail: u16004664@tuks.co.za<sup>\*</sup>; george.markou@up.ac.za<sup>†</sup>

---

9           **Abstract**

10           *Nonlinear dynamic modelling of full-scale wind turbine structures and soil-structure*  
11           *interaction considerations using the 3D detailed approach is the most accurate method of*  
12           *investigating the mechanical response of these structures, but not yet feasible due to numerous*  
13           *reasons. The two main numerical problems that do not allow for this type of analysis to be*  
14           *performed, are the numerical instabilities that immerse during the dynamic analysis and the*  
15           *excessive computational demand. This work will present the computational response of a newly*  
16           *developed algorithm that is used herein to perform modal analysis of wind turbine structures*  
17           *for the investigation of soil-foundation-structure interaction phenomenon. An extensive*  
18           *numerical investigation is presented that foresees the performance of modal and pushover*  
19           *analysis on a wind turbine structure that has an 80 m steel tower and is founded on different*  
20           *soil profiles. The 3D detailed models constructed herein consider the effect of soil-foundation-*  
21           *structure interaction by discretizing for the first time the superstructure, pile foundation and*  
22           *soil domains through 8-noded hexahedral elements, achieving maximum modelling accuracy.*  
23           *The soil material properties used in this research work derived from an onsite geotechnical*  
24           *investigation performed for the needs of the WindAfrica project. After validating the ability of*  
25           *the proposed modelling approach to capture the mechanical behaviour of reinforced concrete*  
26           *foundations through the use of experimental data found in the international literature, the*  
27           *optimum inclination of battered piles was studied through an excessive numerical parametric*  
28           *investigation. Based on the numerical findings, the optimum inclination of the battered piles*  
29           *was that of 10 degrees, where the failure of the wind turbine structure was found to be located*  
30           *at the base of the steel tower due to local buckling.*

31           **Keywords:** Wind Turbines; Soil-Structure Interaction; Battered Piles; Pushover Analysis,  
32           Modal Analysis; Large-Scale Numerical Models.

## 1 INTRODUCTION

2 The modelling of large-scale reinforced concrete (RC) structures by using the finite element  
3 method (FEM) is the most commonly used numerical approach by professionals in the industry,  
4 as well as for research purposes. State-of-the-art finite element (FE) models are constructed by  
5 engineers to investigate the mechanical behaviour of structural designs across all spectrum of  
6 structural types. It is well known that capturing the nonlinear dynamic behaviour of RC  
7 structures through objective and accurate 3D detailed models is a very challenging task [1-3],  
8 whereas taking into account the soil-structure interaction (SSI) effect in an accurate manner [4-  
9 6], constitutes an even more challenging problem due to the computational demands and  
10 numerical instabilities that immerse during both monotonic and cyclic loading scenarios.

11 In addition to the above, one of the structures that scientists cannot study within laboratory  
12 facilities, is that of the wind turbine structures, where due to their sizes, investigating their  
13 mechanical performance through contacting ultimate limit state tests, due to the cost  
14 implications, is not a feasible option. Through time, to obtain more energy, wind turbines  
15 evolved rapidly in height and rotor size, where this growth increased the probability that SSI  
16 effects may influence their structural response. SSI and soil-foundation-structure interaction  
17 (SFSI) considerations are important because of the significant influence they may have on the  
18 structure itself, therefore, ignoring the substructure and the effect it has on the superstructure  
19 can lead to unsafe designs or the development of unanticipated damages. There have been  
20 different numerical methods that were developed to account for the SSI effect without  
21 discretising the soil domain, like the direct integrity method used to model the effect of the soil  
22 on piles through springs and dampers [7, 8]. The springs and dampers approach is used by  
23 many researchers and engineers to construct models for SSI and SFSI investigations, but  
24 nonetheless, this approach is found to be very simplistic and therefore a more accurate approach  
25 was adopted in this research work, that foresaw the development of detailed models with the  
26 use of hexahedral elements for discretizing all domains of the at hand problems.

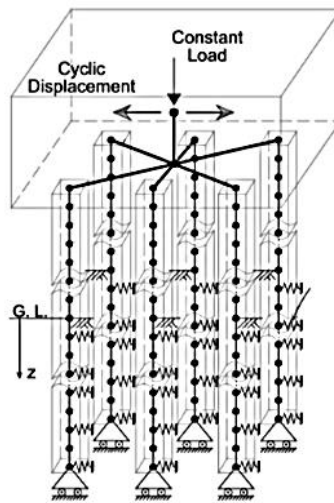
27 When dealing with the study of the mechanical response of structures, it is of great  
28 importance for professionals to be able to predict the natural frequency of wind turbine  
29 structures, therefore, developing a numerical tool for simulating the SFSI effect in detail is of  
30 significant importance. Modelling and analysis of onshore wind turbine structures was  
31 conducted herein through 3D detailed modelling approach [1-4] that was found to be both  
32 efficient and objective, in order to investigate their dynamic response by accounting for an  
33 accurate soil discretization through solid FEs. The soil parameters and wind turbine tower  
34 design used to develop the numerical models were according to the data provided by the  
35 WindAfrica research project [9] that deals with the investigation of wind turbines founded on  
36 expansive clays.

37 In this manuscript, the background and recent research work on SSI will be discussed, where  
38 a summarized description of wind turbine structures will be presented. The proposed modeling  
39 method will also be presented, where the basic features of concrete, steel and soil material  
40 modeling will be given. The validation of the proposed numerical modeling approach will be  
41 discussed, while the numerical investigation campaign will be presented through discussing  
42 the developed models. Finally, the numerical results based on the modal and push over  
43 analyses, whereas the final conclusions will be given.

1 **2 CURRENT KNOWLEDGE AND MODELING CONSIDERATIONS**

2 **2.1 SOIL-STRUCTURE INTERACTION PHENOMENON**

3 The SSI is a complex phenomenon, which lies at the intersection of the soil and structure.  
 4 When dealing with large-scale structures such as wind turbines, the effects can be significant  
 5 especially in cases where the soil is of poor material properties (i.e. soft clay that has a small  
 6 E-value). As it was discussed above, there are different numerical methods that were developed  
 7 to study the SSI phenomenon, like the direct integrity method used to model the effect of the  
 8 soil on piles through springs and dampers [7, 8]. Nonetheless, an approach that is gaining more  
 9 popularity over the past decade as the computational efficiency of personal computers increases  
 10 is the three-dimensional modelling approach, which is a method that has a large computational  
 11 demand but yields the most accurate results.



12

13 Figure 1 Spring and damper approach of the Quasi-Static Cyclic Test [10].

14 The SSI phenomenon was investigated by Wang *et al.* [10] (Fig. 1), where they performed  
 15 and studied several SSI experiments on piled foundations. It must be noted that their project  
 16 did not only consist of experiments but also numerical analyses in an attempt to compare the  
 17 numerically and experimentally obtain data. The numerical analyses performed by Wang *et al.*  
 18 [10] used the spring and damper approach to capture the overall mechanical behaviour of the  
 19 structure. The test foresaw performing a cyclic analysis on a pile foundation with six  
 20 rectangular piles embedded in sand, while the soil was simulated with springs [10] and the  
 21 different parameters with the increase of depth were based on values found in Blanco *et al.*  
 22 [11]. The piles were modelled by using beam-column FEs and they were assumed to be pinned  
 23 at the bottom preventing any displacement or uplift during the numerical analysis. This  
 24 numerical strategy decreases the lateral displacement during loading, a numerical assumption  
 25 that contradicted with the actual physical test that foresaw the placement of sand under the tips  
 26 of the piles. Furthermore, more research on offshore wind turbine structures supported by  
 27 monopiles was done by several researchers [12-16].

28 It must be noted here that the specimen in Fig. 1 was used to validate the ability of ReConAn  
 29 FEA [17] in reproducing experimental results and capture the SSI effects (Section 3). ReConAn  
 30 FEA is the software that was adopted for the needs of this research work.

## 2.2 PILE FOUNDATIONS

The most used onshore wind turbine structure foundation is the pile foundation. This method is used to obtain stability through the bedrock and reduce the distributed forces in the underlying soil. Also, the contact area of the pile-cap with the soil reduces the stresses on the underlying soil domain, whereas the cost of the foundation depends on the depth of the piles, which relates to the geological condition of the under-study ground. There are various pile shapes and sizes, which includes inclination of piles relative to the vertical axis (battered piles). Battered piles can be used to provide with additional stability to large RC structures during horizontal loading conditions, whereas the piles can be designed to have a certain angle of inclination.

Based on the work of Vu *et al.* [18], by implementing battered piles the horizontal stiffness of the structure increases relative to the horizontal displacements. This research entailed of many experiments and numerical analyses, following the influence of battered piles on the horizontal stiffness and displacement of piles. The conclusion made during their study [18] was that a pile inclination of 15 degrees improves the horizontal resistance by decreasing the lateral displacement under horizontal loading, due to the observed overall increased stiffness. Their performed test, which involved connected and unconnected pile rafts, yielded a small increase in horizontal stiffness when the piles were connected to the raft, where the vertical stiffness resulted into a relatively low resistance when the piles weren't connected to the raft [18].

In addition to the above, by implementing negative and positive angles of inclined battered piles can also have a large influence on the dynamic behaviour of the structure. Additional research on the previous mentioned phenomenon was conducted by Rajashree and Sitharam [19]. The research covered the analysis of a pile embedded in soft clay with a raft support at the bottom of the pile. Their analyses included pile inclinations of -30, -10, 0, 10 and 30 degrees (a positive angle was taken as anticlockwise from the vertical axis). As reported, the angle with 30 degrees yielded more lateral resistance, whereas the experiment did not only report better results for the positive pile inclinations, but also more resistance in comparison to the vertical pile configuration.

## 2.3 MODAL AND NONLINEAR ANALYSIS OF WIND TURBINE STRUCTURES

Based on the work published by Prowell *et al.* [20], the influence of the SSI on wind turbine structures was investigated. The research conducted in [20] involved a modal analysis of a 5 MW wind turbine structure considering SSI effects. The analyses consisted of a wind turbine structure that was discretized by beam-column FEs and a large soil mesh that foresaw the use of solid FEs. The foundation consisted of a monopile that was created by filling a hollow steel tube with concrete, while the soil parameters that were assumed during the analysis foresaw a stiff, medium and soft soil domain. According to their numerical investigation, the natural frequencies, maximum bending moments and shear forces due to seismic actions were measured. As it was reported [20], the numerical results that were obtained derived an increase in natural frequency as the soil became stiffer with a larger influence of the SSI found when the soil was softer. Furthermore, a pushover analysis of a 53 m high wind turbine structure was conducted by Guo *et al.* [21]. In this work, the wind turbine tower was divided into 9 segments, and was studied using two types of analyses. The first was a pushover analysis that assumed for the dead loads and the second accounted for the seismic load only.

Within this manuscript, numerous 3D detailed models were created, where modal analysis was performed to get an overview of the expected structures' dynamic response. Referring to natural frequencies and eigenmodes, where engineers will be able to establish that periodic excitations and avoid resonance phenomena that may lead to the development of

1 excessive stresses and strains. Mass is also a controlling parameter when dealing with heavy  
 2 or light structures, thus, the investigation results that will be presented in the following section  
 3 assumes the detailed representation of the frame's geometry and structural masses.

4 There are several solution methods for solving the eigenvalue problem that is described by  
 5 the following equation:

$$6 \quad \mathbf{K}\boldsymbol{\phi}_i = \lambda_i \mathbf{M}\boldsymbol{\phi}_i \quad (1)$$

7 where,  $\mathbf{K}$  is the stiffness matrix of the model,  $\mathbf{M}$  is the mass matrix of the model,  $\boldsymbol{\phi}_i$  is a vector  
 8 that contains the eigenvectors of the system and  $\lambda_i$  is the corresponding eigenvalue  $i$ . The  
 9 solution method used in this research work is called the subspace iteration algorithm [22]. This  
 10 solution technique is ideal when dealing with large-scale structures since it calculates few  
 11 eigenvalues and eigenvectors of a significantly computationally demanding FE model.

12 This solution algorithm finds an orthogonal basis of vectors in  $\mathbf{E}_{K+1}$ , calculating in one step  
 13 the required eigenvectors when  $\mathbf{E}_{K+1}$  converges to  $\mathbf{E}_\infty$ . The developed algorithm foresees the  
 14 iteration used in the subspace iteration method, i.e., step 2 of the complete solution phase  
 15 proposed by Bathe [22]. For  $k = 1, 2, \dots$ , iterate from  $\mathbf{E}_k$  to  $\mathbf{E}_{k+1}$ :

$$16 \quad \mathbf{K}\mathbf{X}_{k+1} = \mathbf{M}\mathbf{x}_k \quad (2)$$

17 then, find the projections of matrices  $\mathbf{K}$  and  $\mathbf{M}$  onto  $\mathbf{E}_{k+1}$ :

$$18 \quad \mathbf{K}_{k+1} = \mathbf{X}_{k+1}^T \mathbf{K} \mathbf{X}_{k+1} \quad (3)$$

$$19 \quad \mathbf{M}_{k+1} = \mathbf{X}_{k+1}^T \mathbf{M} \mathbf{X}_{k+1} \quad (4)$$

20 and solve for the eigensystem of the projected matrices:

$$21 \quad \mathbf{K}_{k+1} \mathbf{Q}_{k+1} = \mathbf{M}_{k+1} \mathbf{Q}_{k+1} \boldsymbol{\Lambda}_{k+1} \quad (5)$$

22 Thereafter, find an improved approximation to the eigenvectors:

$$23 \quad \mathbf{x}_{k+1} = \mathbf{X}_{k+1} \mathbf{Q}_{k+1} \quad (6)$$

24 and then provided that the vectors  $\mathbf{x}_1$  are not orthogonal to one of the equilibrium eigenvectors,  
 25  $\boldsymbol{\Lambda}_{k+1} \rightarrow \boldsymbol{\Lambda}$  and  $\mathbf{X}_{k+1} \rightarrow \boldsymbol{\Phi}$  as  $k \rightarrow \infty$ .

26 It is important to note that the convergence of this method assumes that within the iteration  
 27 procedure the vectors in  $\mathbf{X}_{k+1}$  are ordered in such a way that the  $i^{\text{th}}$  diagonal element in  $\boldsymbol{\Lambda}_{k+1}$   
 28 is always larger than the previous  $i-1$  element,  $i=2, \dots, p$ . This ensures that the  $i^{\text{th}}$  column in  
 29  $\mathbf{X}_{k+1}$  converges linearly to  $\boldsymbol{\Phi}_i$ . Although this is an asymptotic convergence rate, it was found  
 30 that the smallest eigenvalues converge fastest [22], a finding confirmed by the authors of this  
 31 manuscript through their work that was published in [23, 24]. This algorithm is adopted herein  
 32 for the needs of this research work.

33 Given that the 3D detailed modeling approach foresees the use of hexahedral elements for  
 34 the discretization of the concrete medium (3D elements) and simulates the reinforcement with  
 35 embedded rebar elements (1D elements), the material models use a 3D and 1D formulations,  
 36 respectively. Therefore, the modal analyses performed herein make use of the material values  
 37 based on the exact 3D mesh of each model.

## 2.4 MATERIAL CONSTITUTIVE MODELS OF REINFORCED CONCRETE AND SOIL

As discussed in the work performed by Mourlas *et al.* [25], the constitutive modelling of concrete must describe the realistic behavior of concrete under generalized 3D states of stress. Therefore, it must consider the effect of out-of-plane stresses that are usually ignored when 1D and 2D material models are used. According to the adopted 3D material model for concrete, it is assumed that the uncracked concrete behaves as an isotropic material. The strain-softening stress-strain descending branch, which appears at most uniaxial constitutive models in compression, is attributed to the interaction between the specimen and the loading platens [26], therefore, it is not accounted for in this study. As it was shown in previous research works [4, 23, 27 - 30], the ductile behavior of RC members and full-scale structures can derive from the interaction between concrete and the steel reinforcement.

In order to describe the stress-strain relationships, each state of strain and stress are decomposed into hydrostatic and deviatoric components. Therefore, the normal and shear octahedral stresses ( $\sigma_0$ ,  $\tau_0$ ) and strains ( $\varepsilon_0$ ,  $\gamma_0$ ) are used to form their constitutive relationships. The hydrostatic stresses  $\sigma_0$  induce the variation of the volumetric strain  $\varepsilon_{0(h)}$ , while the application of deviatoric stresses  $\tau_0$  cause the development of both volumetric and deviatoric strains. The combined approach presented by Kotsovos and Pavlovic [26] is based on the use of the bulk modulus  $K$  and the shear modulus  $G$ , which describe the non-linear  $\sigma_0$ - $\varepsilon_{0(h)}$  and  $\tau_0$ - $\gamma_{0(d)}$  behavior combined with the use of the  $\sigma_{id}$  stress in order to take into account the coupling effect of  $\tau_0$ - $\varepsilon_{0(d)}$  ( $h$  and  $d$  stand for hydrostatic and deviatoric components, respectively). The  $\sigma_{id}$  stress is an equivalent external stress which can be added to the externally applied hydrostatic stress. Then, the constitutive relations take the following form:

$$\varepsilon_0 = \varepsilon_{0(h)} + \varepsilon_{0(d)} = (\sigma_0 + \sigma_{id}) / (3K_s) \quad (7)$$

$$\gamma_0 = \gamma_{0(d)} = \tau_0 / (2G_s) \quad (8)$$

where  $K_s$  and  $G_s$  is the secant forms of the bulk and shear modulus, respectively. An extensive experimental investigation in [26] led to the analytical expressions of the  $\sigma_{id}$  stress and the secant and tangent forms of the bulk and shear moduli as functions of the current state of stress ( $\sigma_0$ ,  $\tau_0$ ,  $f_c$ ).

The strains in global coordinates are determined using Eq. (9) that takes the following equivalent form:

$$\varepsilon_{ij} = (\sigma_{ij} + \sigma_{id}\delta_{ij}) / (2G_s) - (3\nu_s / E_s)(\sigma_0 + \sigma_{id})\delta_{ij} \quad (9)$$

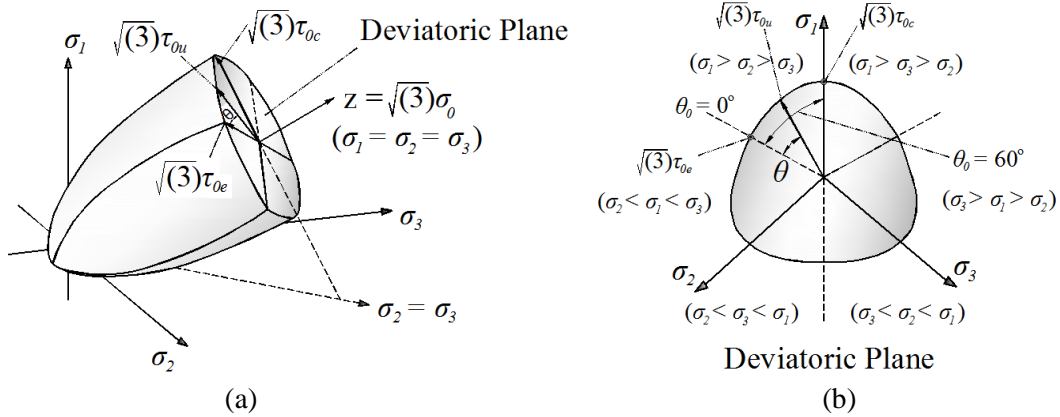
where  $E_s$  ( $\sigma_0$ ,  $\tau_0$ ,  $f_c$ ) and  $\nu_s$  ( $\sigma_0$ ,  $\tau_0$ ,  $f_c$ ) are the secant Young's modulus and Poisson's ratio, respectively, derived from  $K_s$  and  $G_s$  by the following standard formulae of linear elasticity:

$$E_s = (9K_s G_s) / (3K_s + G_s) , \nu_s = (3K_s - 2G_s) / (6K_s + 2G_s) \quad (10)$$

During the nonlinear procedure, the stress and strain increments are calculated using the tangent expressions of modulus  $K_t$ ,  $G_t$ ,  $E_t$ ,  $\nu_t$ . The expression in Eq. 11 of the strength envelope of concrete is formulated based on the Willam and Warkne (1974) formulae and adopted in this research work. Furthermore, Fig. 2 shows the graphical illustration of the adopted ultimate surface for concrete. It must be noted at this point that, the concrete material model was modified algorithmically in [27] so as to improve its numerical response by alleviating numerical instabilities. The proposed algorithmic enhancement [27] is adopted for the needs of

1 this research work.

$$\tau_{0u} = \frac{2\tau_{0c}(\tau_{0c}^2 - \tau_{0e}^2)\cos\theta + \tau_{0c}(2\tau_{0e} - \tau_{0c})\sqrt{4(\tau_{0c}^2 - \tau_{0e}^2)\cos^2\theta + 5\tau_{0e}^2 - 4\tau_{0c}^2\tau_{0e}^2}}{4(\tau_{0c}^2 - \tau_{0e}^2)\cos^2\theta + (2\tau_{0e} - \tau_{0c})^2} \quad (11)$$

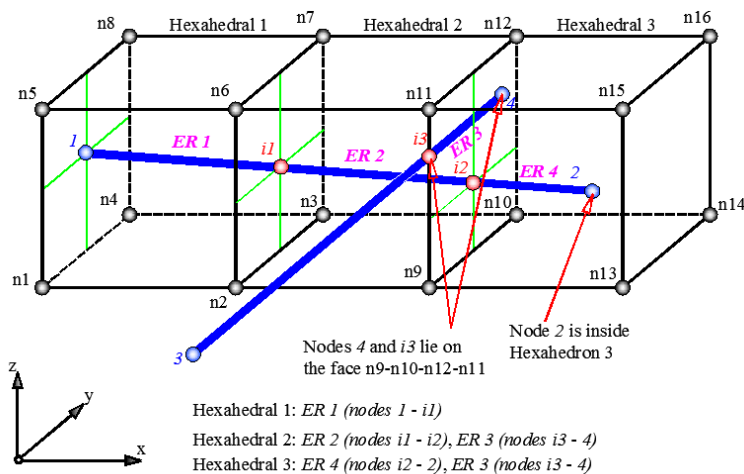


2  
3  
4  
5

Figure 2 Ultimate-strength surface based on the adopted failure criterion. (a) 3D view of the surface; (b) Cross-section of the strength envelope coinciding with a deviatoric plane. [31]

6 In terms of reinforcement modeling, when simulating large-scale RC structures, it is  
7 essential to model the embedded rebar elements with a unique and efficient method. The  
8 reinforcement is simulated as a uniaxial element without considering the shear and bending  
9 stiffness, however there are cases where the shear and bending stiffness are important in  
10 capturing the nonlinear response of the RC members [27].

11 Previous research performed by Markou and Papadrakakis [27, 31] showed that by using  
12 hexahedral elements for discretizing the concrete domain and Natural Beam-Column  
13 Flexibility-Based (NBCFB) elements as embedded rebars the numerical stability of the  
14 nonlinear procedure was improved. When a NBCFB element is used to model reinforcement  
15 within a hexahedral mesh, the rotation of the hexahedral faces and the rotation of the rebar  
16 nodes that are located on the corresponding hexahedral faces, must be enforced [27, 31].



17  
18

Figure 3 Embedded reinforcement rebars inside hexahedral elements. [31]

19 The method proposed by Markou and Papadrakakis [27, 31], where the main objective of  
20 was to reduce the computational cost regarding the generation of the embedded reinforcement,  
21 enabled the mesh generation procedure to be applicable for large-scale FE models with a

1 significant number of embedded rebar elements, while more research followed in [32] where  
 2 large-scale RC structures were investigated. The proposed embedded rebar mesh generation in  
 3 [27, 31] considers arbitrary positioning of the rebars inside the concrete elements, as shown in  
 4 Fig. 3, while avoiding a nonlinear search procedure for the calculation of the natural  
 5 coordinates of the embedded reinforcement nodes in the corresponding prismatic hexahedral  
 6 elements. By separating the generation algorithm into two main parts, the geometry of each  
 7 hexahedral element is categorized (prismatic or non-prismatic) and accordingly treated in order  
 8 to compute the natural coordinates of its containing embedded rebar elements [27, 31].

9 It must be noted here that the material of steel-reinforcement is modeled through the use of  
 10 the Menegotto-Pinto [33] model that considers the Bauschinger effect. The stress-strain  
 11 relation takes the form:

$$\sigma^* = b\varepsilon^* + \frac{(1-b)\varepsilon^*}{(1+\varepsilon^{*R})^{1/R}} \quad (12)$$

12 where  $\varepsilon^* = (\varepsilon - \varepsilon_r) / (\varepsilon_0 - \varepsilon_r)$ ,  $\sigma^* = (\sigma - \sigma_r) / (\sigma_0 - \sigma_r)$  and  $R = R_0 - \frac{a_1\xi}{a_2 + \xi}$

13 The parameter b is the strain hardening ratio between  $E_0$  and  $E_t$ ,  $\varepsilon_0$  and  $\sigma_0$  are the coordinates  
 14 of the point where the asymptotes of the branch intersect,  $\varepsilon_r$  and  $\sigma_r$  are the coordinates of the  
 15 point where the last strain reversal with stress of equal sign takes place. The parameter R is a  
 16 decreasing function of  $\xi$ , which is the strain difference between the current asymptote  
 17 intersection point and the previous load reversal point with maximum or minimum strain,  
 18 depending on whether the corresponding steel stress at reversal is positive or negative.  $R_0$ ,  $a_1$   
 19 and  $a_2$  are experimentally determined parameters and assumed to be 20, 18.5 and 0.15,  
 20 respectively in this study.

21 For the case of the SSI models that foresaw the discretization of the soil domain through the  
 22 use of hexahedral elements, the soil material model foresaw the adoption of a nonlinear  
 23 elastoplastic 3D material model that assumed a von Mises yielding criterion (see Eq. 13). The  
 24 analysis that is performed in this work foresees that the wind turbine structures are founded on  
 25 unsaturated clay soil. The adopted material model requires only three material properties to be  
 26 defined, the E-value, Poison Ratio and the uniaxial ultimate stress of the soil. A typical von  
 27 Mises yielding criterion curve can be seen in Fig. 4.

$$(\sigma_1 - \sigma_3)^2 - (\sigma_1 - \sigma_3)(\sigma_2 - \sigma_3) + (\sigma_2 - \sigma_3)^2 = \sigma_y^2 \quad (13)$$

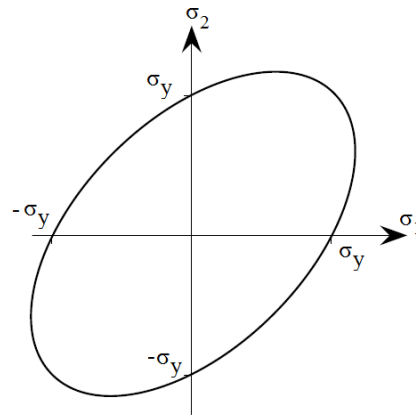
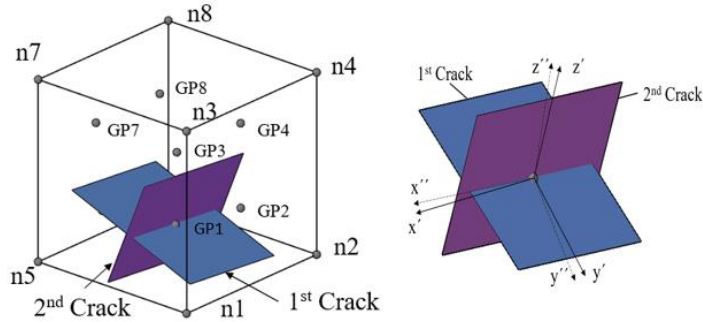


Figure 4: von Mises 2D yielding criterion curve.

1 **2.5 SMEARED CRACK APPROACH**

2 The first to introduce this approach was Rashid [34] who studied prestressed concrete  
 3 pressure vessels. This approach is numerically simple, and it can be used in any nonlinear FE  
 4 code by constructing a routine for the newly developed material constitutive model, avoiding  
 5 the need of re-meshing to capture the cracks.



6  
 7 Figure 5 Local axes for the case of two cracks at a specific Gauss point [25].

8 The smeared crack approach foresees the modification of the stiffness matrix and stresses  
 9 at corresponding integration points, therefore, the approach consists of simulations of  
 10 individual cracks (Fig. 5) without remeshing. The prediction of the direction of propagation is  
 11 based on the failure criterion that is expressed in terms of stresses (see Eq. 11). The conclusion  
 12 can be made that remeshing is not necessary when using this approach as the smeared crack  
 13 model does not consider discontinuities in the topology of the FE mesh.

14 When the failure criterion is satisfied, then a crack plane is assumed to form in the direction  
 15 orthogonal to the maximum principle tensile stress (see Fig. 5). Cracking is modeled by the  
 16 smeared-crack approach in which the stiffness corresponding to the direction of the maximum  
 17 principle tensile stress is set to zero by transforming the constitutive matrix of the material.  
 18 Assuming that the crack is perpendicular to  $z'$  axis the constitutive matrix takes the following  
 19 form:

$$\mathbf{D} = \begin{bmatrix} 2G_t + \mu & \mu & 0 & 0 & 0 & 0 \\ \mu & 2G_t + \mu & 0 & 0 & 0 & 0 \\ 0 & 0 & 0 & 0 & 0 & 0 \\ 0 & 0 & 0 & G_t & 0 & 0 \\ 0 & 0 & 0 & 0 & \beta G_t & 0 \\ 0 & 0 & 0 & 0 & 0 & \beta G_t \end{bmatrix} \quad (14)$$

20 This expression of the constitutive matrix describes anisotropic behavior of concrete in the  
 21 local axis. Therefore, the constitutive matrix has to be transformed to global axes using the  
 22 standard coordinate system transformation law as follows:

$$\mathbf{D}_{gl} = \mathbf{T}^T \mathbf{D} \mathbf{T} \quad (15)$$

23 where  $\mathbf{T}$  is the transformation matrix from the local Cartesian system  $(x', y', z')$  to a global  $(x,$   
 24  $y, z)$  with the direction cosines given by  $(l_i, m_i, n_i)$  which define the relative orientation of  $i$ -  
 25 axis of system  $(x', y', z')$  to  $(x, y, z)$ , respectively. For more details on the smeared crack  
 26 approach please refer to [27, 31].

### 3 PARAMETRIC VALIDATION OF THE PROPOSED MODEL

The experiment performed by Wang *et al.* [10] was investigated in this section to validate the proposed SFSI modelling approach. The model was used to validate the SSI of concrete piles, which are subjected to vertical and lateral loading. The experimental test was simulated herein through a pushover analysis. The experiment of Wang *et al.* [10] was performed by inducing cyclic loading through the use of an actuator, however, for the scope of this work, a single pushover analysis was conducted to produce the P- $\delta$  curve and study the respective failure mechanism, thus investigate the ability of the proposed model in capturing the envelop curve. The dimensions of the numerical model can be seen in Figs. 6 and 7.

Sand can not resist tensile forces and therefore, the model was constructed in such a manner (see Fig. 8), where the tensile resistance of the soil was adjusted accordingly based on the location around the piles. The rebars that were used to construct the piles foresaw an 8 mm in diameter rebar for stirrups and 12 mm for the longitudinal rebars (see Fig. 8). As reported by Wang *et al.* [10], the pilecap was subjected to vertical loads by lead bricks and therefore, the pilecap was also included in the developed model on which a distributed load based on the total experimentally applied load was imposed.

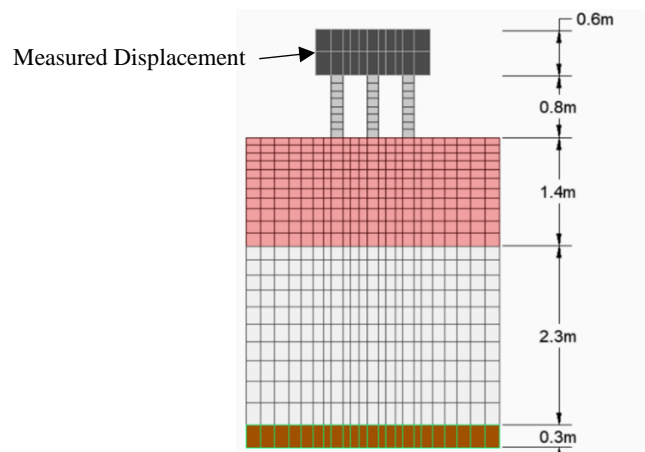


Figure 6 Front view illustrating the dimensions of the numerical model.

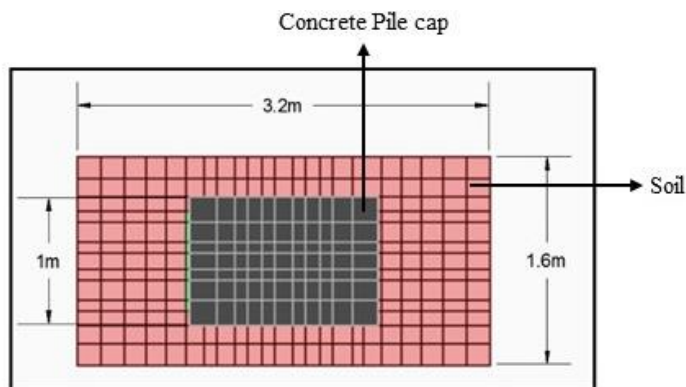
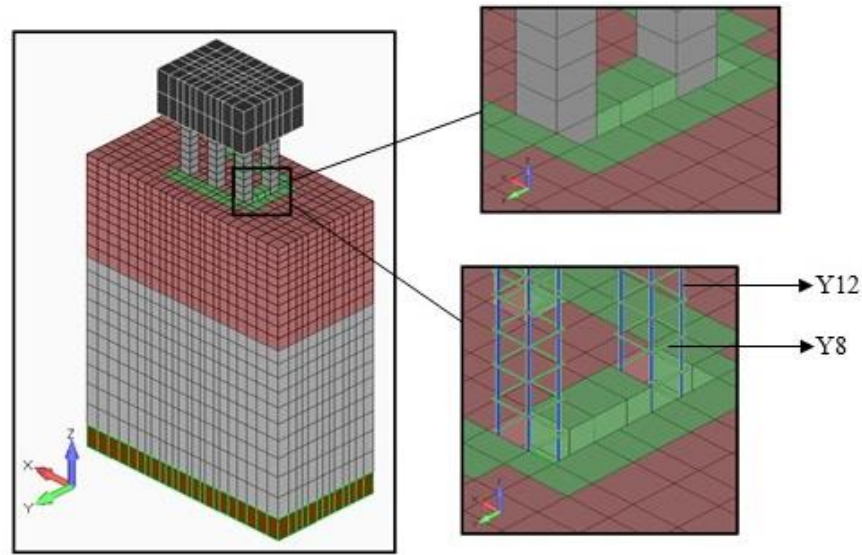


Figure 7 Top view illustrating the dimensions of the hexahedral mesh of the model.

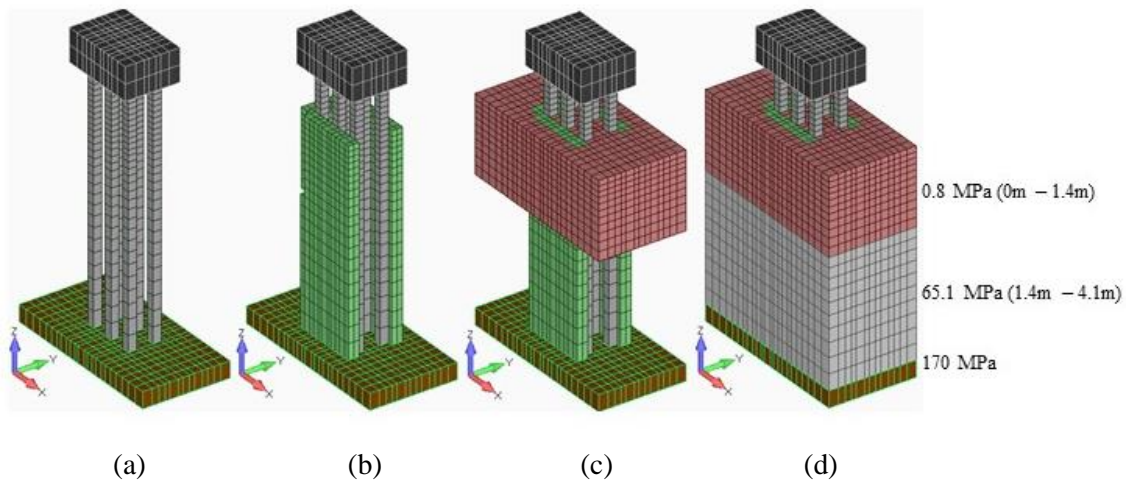


1

2

3

Figure 8 Finite element mesh of the model with piles and a pile cap. Hexahedral and embedded rebar element.



4

5

6

Figure 9 Modelling of the different soil regions of the specimen.

7

8

9

10

11

12

13

14

15

16

17

18

19

20

21

22

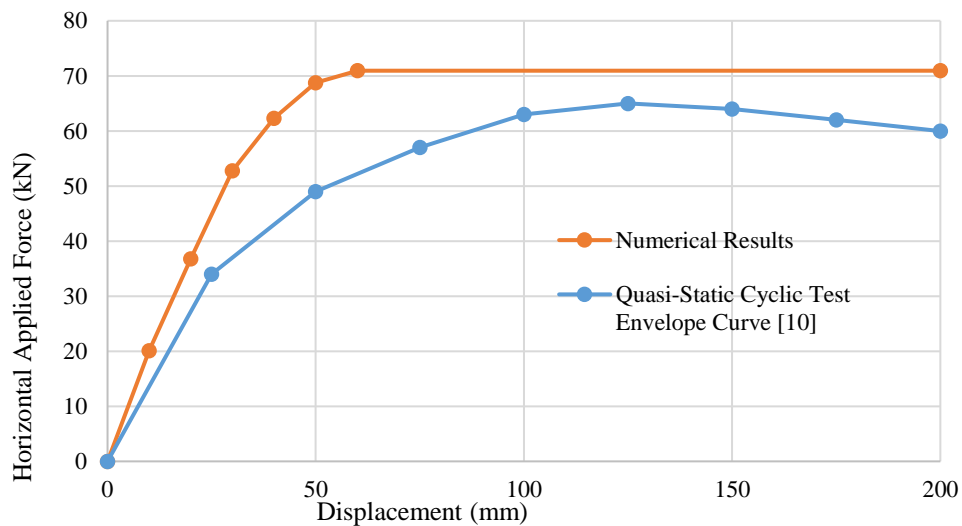
The soil geometry was refined to simulate the conditions of the experiment as accurately as possible. The soil layer at the bottom of the container shown in Fig. 9a, was modelled to behave as a relatively stiff base that, nevertheless, allows movement in all directions (deformable). The E-value, as well as the limiting compression stress assumed during the numerical nonlinear analysis are given in Table 1. The primary soil was divided into two separate soil layers (see Fig. 9d). The top soil layer had an E-value that is smaller due to lower compaction and stress levels, as the bottom layer will have a higher E-value due to compaction of the overlain material. It is also noteworthy to state here that, the nodes found at the soil's perimeter were allowed to settle along the z-global axis, while their x and y degrees of freedom were restrained. The base of the soil domain was assumed to be fixed. The values in Table 1 were assumed based on the experiment performed by Wang *et al.* [10].

The numerical results were compared with the envelop curve as it derived from the experimental data (see Fig. 10). The numerical results are found to be in a good agreement with the corresponding experimental data, whereas the numerical model was found to behave in a stiffer manner. This numerical response was expected, as during the experiment performed by Wang *et al.* [10] a cyclic loading test was conducted and in the numerical modelling performed

1 herein only a pushover analysis was performed. It is evident that the cyclic loading of the  
 2 specimen caused the weakening of concrete through the opening and closing of cracks,  
 3 resulting into an overall resistance decrease (see Fig. 10). Therefore, it is safe to conclude that  
 4 the proposed modeling approach is able to capture the mechanical behavior of the RC  
 5 foundation in a realistic manner.

6 Table 1 E-value and compression strength of the assumed soil materials.

Material	Description/colour	E-value (MPa)	Limit compression stress (MPa)
Concrete	Grey	20,000	29
Steel	Reinforcement	200,000	335
Soil	0-1.4 m, Maroon	0.8	0.05
	1.4-4.1 m, Grey	65.1	0.015
	Around the sides of piles	0.01	0.01
	Base layer, Brown	170	4.5



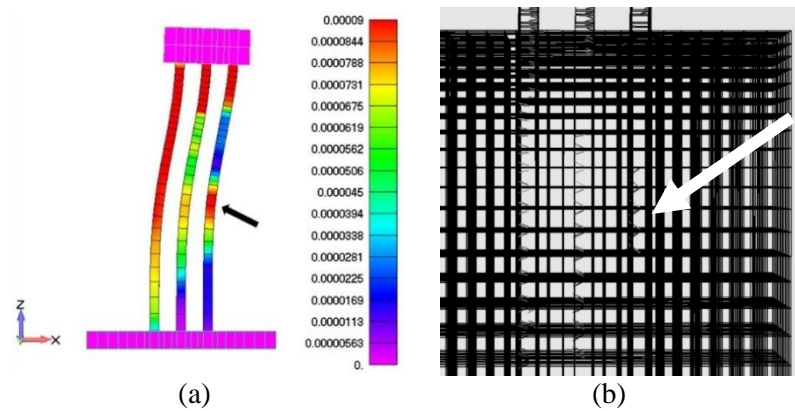
7

8 Figure 10 SSI RC specimen. Comparison of the numerical and experimental curves.

9 The solid von Mises Strains were visualized at the step where cracks start to propagate in  
 10 the concrete domain. These strains were compared to the actual crack formation in the  
 11 concrete piles (see Figs. 11 and 12) in order to investigate the ability of the model to predict  
 12 the regions of crack development. The crack formation was found to be in a good agreement  
 13 with the experimentally observed crack patterns (see Fig. 13), illustrating the ability of the  
 14 developed model to reproduce both the overall mechanical behaviour of the specimen and the  
 15 damages developed at the local level. Based on the Wang *et al.* [10] research work, it was  
 16 reported that the first cracks occurred at the piles near the joint with the pile cap (Fig. 13b).  
 17 The numerical findings not only verified this experimental observation, but also revealed that  
 18 the pile cracking occurred (at the same time) at the middle of the pile's height (see Fig. 11b),  
 19 something that could not be observed during the physical experiment due to the fact that the  
 20 piles were covered with sand.

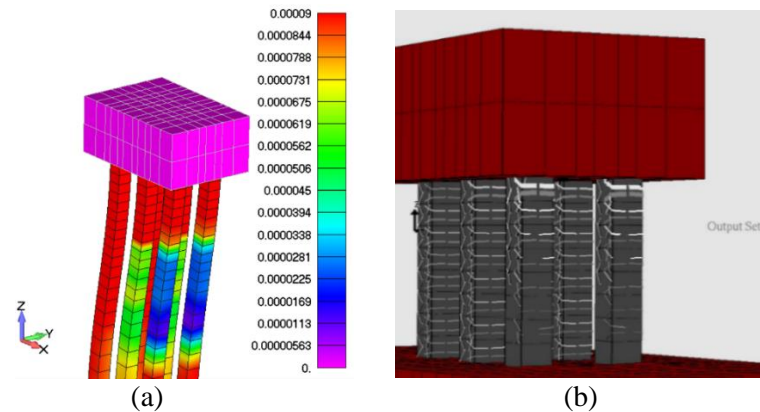
21 The stress distribution can be seen in Fig. 14a for the top soil layer, Fig. 14b for the middle  
 22 soil layer and Fig. 15a for the hard-bottom soil layer as they resulted from the numerical

1 analysis. The stress contour legend is measured in kPa. The stress distribution yielded an  
2 exceedance of the soil limit compression stress around the piles. However, as expected the  
3 stress decreased further away from the piles.



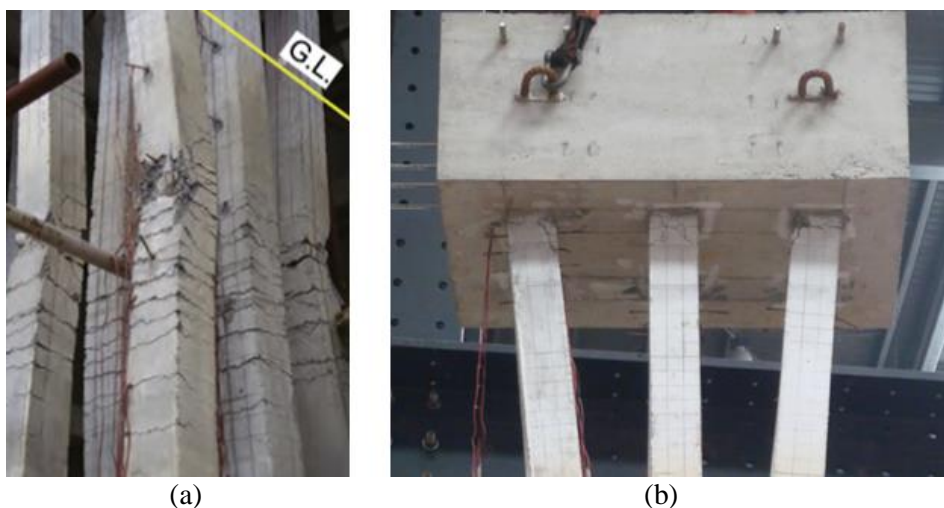
4  
5  
6  
7

Figure 11 Front view crack formation in the piles. (a) Solid von Mises Strains of the concrete piles and (b) Crack formation of the concrete piles.



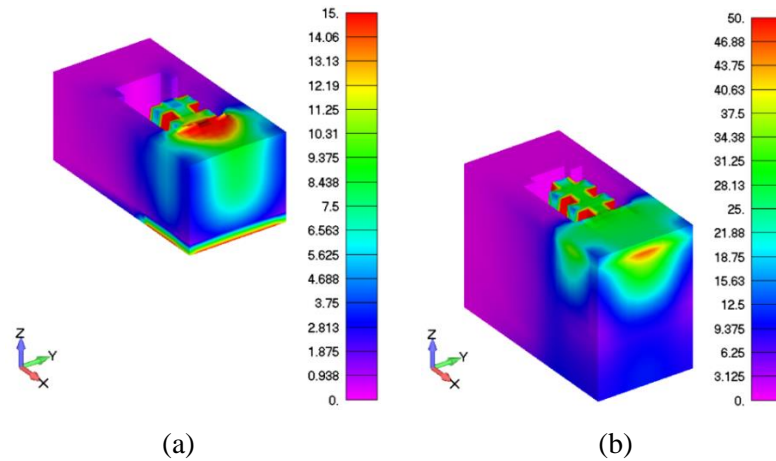
8  
9  
10  
11

Figure 12 Front view of the deformed shapes of the piles. (a) Solid von Mises Strains of the concrete piles and Pile cap and (b) Crack formation of the concrete piles.



12  
13  
14  
15

Figure 13 Crack formation in the piles of the Wang *et al.* [10] experiment. (a) Crack formation in the middle of the piles and (b) Crack formation at the pile cap connection as found in [10].

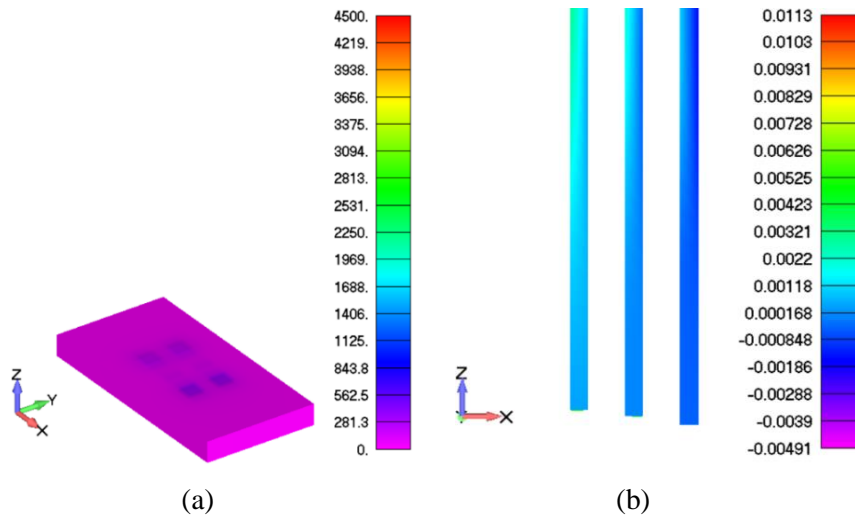


1  
2  
3

Figure 14 Solid von Mises Stress distribution. (a) Top soil and (b) Middle soil layers (kPa).

4 The stress distribution showed in Fig. 15a produced a high compression stress in the hard-  
5 bottom layer. The two front pile developed a settlement (Fig. 14b) that caused a compressive  
6 stress field under their tip. This important phenomenon was neglected by Wang *et al.* [10] when  
7 modeling the foundation, an observation that further illustrates why the spring model that was  
8 developed in their research work had limitations. It is evident (see Fig. 14b) that the piles in  
9 the middle had almost no contribution to the stress distribution in the bottom soil layer, a  
10 phenomenon attributed to the piles that are situated on the neutral axis.

11 It is safe to conclude at this point that, the proposed modeling method does not only have  
12 the ability to capture the overall mechanical behaviour of RC foundations that are affected by  
13 the SSI phenomenon, but it also can provide with valuable inside on the behaviour of the soil  
14 domain and the areas were damages and plastification can occur.



15  
16  
17  
18

Figure 15 (a) Solid von Mises Stress distribution of the hard-bottom soil layer (kPa) and (b) Settlement of the RC piles – scaled deformation ZX View.

1 **4 NUMERICAL INVESTIGATION OF WIND TURBINE**  
2 **STRUCTURES WITH SFSI CONSIDERATIONS**

3 This section will present the models that were developed for the needs of the numerical  
4 investigation performed in this research work, where the results from the mesh sensitivity will  
5 also be discussed. Several soil profiles were investigated that included soil geometries based  
6 on the Wind Africa project [9], whereas soil geometries where the piles are embedded in rock  
7 and situated on softer soil are analysed. During the soil geometry investigation, the pile  
8 inclination was modified to determine the optimal foundation design for the under-study wind  
9 turbine structure. The final selected superstructure geometry is based on 80 m tall typical  
10 VESTA wind turbine structure.

11 Prior to the numerical investigation of the modal analyses, a mesh sensitivity was performed  
12 to derive the optimal FE size. The mesh sensitivity yielded an optimum mesh geometry when  
13 0.5 m hexahedral elements are used. Modal analyses were performed for all the developed  
14 models to investigate the difference in terms of dynamic response by comparing the  
15 numerically obtained eigenmodes and eigenfrequencies. Thereafter, pushover analyses were  
16 performed to further investigate the mechanical performance of the battered pile foundation.

17 Buckling was also considered during the performance of the pushover analyses, while, a  
18 step increment investigation was performed in order to demonstrate the robustness of the  
19 nonlinear solution algorithm incorporated in ReConAn FEA, where the mechanical response  
20 of the structure and the SFSI effects were investigated. Pushover analyses were performed on  
21 the optimal design obtained through the modal analysis, where the battered piles of different  
22 inclination angles were investigated.

23 It must be noted here that, the developed modal algorithm incorporated in ReConAn FEA  
24 [35] and its ability to accurately predict the fundamental modes of RC structures was validated  
25 through the use of experimental data found in the international literature, whereas the validation  
26 was published in [28, 29, 30, 23]. Gravett *et al.* [24] used the developed algorithm in the study  
27 of 2-,4-,6-,8-,10- and 20-storeys RC buildings and their dynamic response, while the algorithm  
28 was also recently used for the investigation of the SSI phenomenon and its effect on the  
29 fundamental period of multi-storey RC structures [6].

30 **4.1 PILE CAP AND TOWER GEOMETRY OF THE WIND TURBINE**  
31 **STRUCTURE**

32 The understudy 2 m thick foundations' pile cap can be seen in Fig. 16, where the piles were  
33 spaced so that the distance between the pile centre and the pile cap centre remained constant in  
34 all models. The steel tower thickness was assumed to be equal to 3 cm, spanning a total conical  
35 height of 80 m. Furthermore, the design of the wind turbine tower was based on a 5 MW design  
36 [9], therefore, the bottom diameter of the tower was 6 m and the top outer diameter 3.87 m (see  
37 Fig. 17).

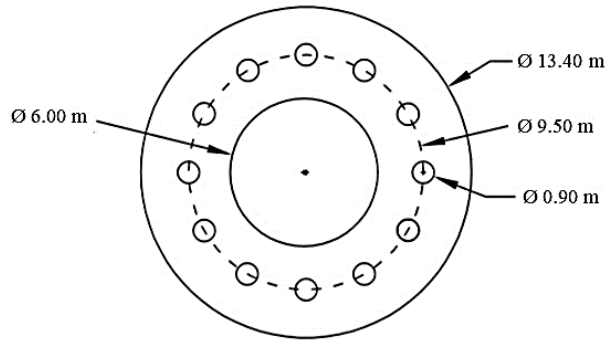


Figure 16 Pile cap geometry (Not to scale).

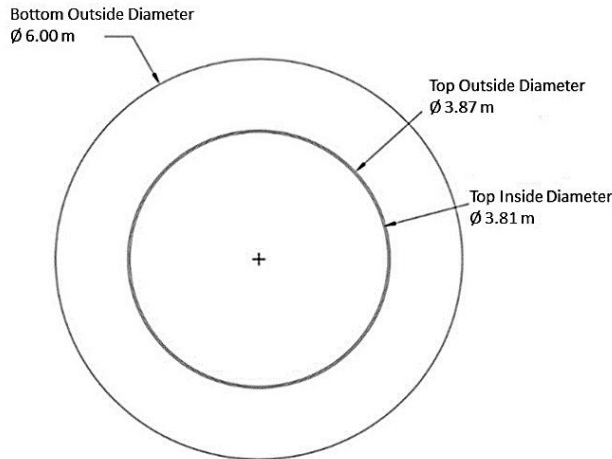


Figure 17 Wind Turbine tower geometry. Plan view.

1  
2

3  
4

5 Initially, two turbine geometries were developed, however, it was decided to consider only  
6 one (based on the needs of the project [9]), where the full structure was discretized in detail  
7 (see Fig. 18). As it can be seen, hexahedral FEs were used to discretize the soil, piles, pile cap  
8 and steel tower of the structure. After performing the modal analyses, it was decided to replace  
9 with a mass load the blades, nacelle and hub (discretized with tetrahedral FEs and the masses  
10 of the several components was added to the structure) to reduce the computational demand of  
11 the model. It must be noted at this point that, for all the modal analyses performed for the needs  
12 of this research study the mass from the Nacelle-Rotor-Assembly was applied at the top of the  
13 tower by increasing the nominal weight of the hexahedral elements found at the last layer at  
14 the tip of the steel tower.

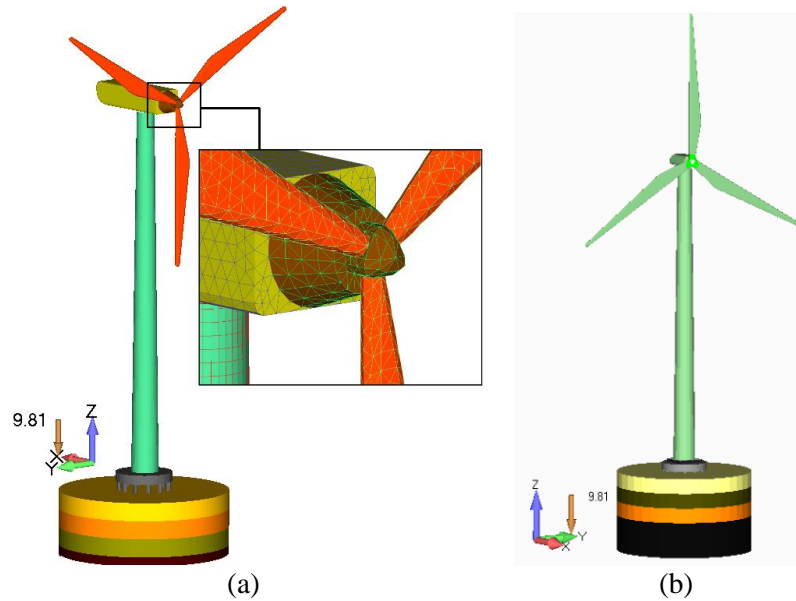


Figure 18 Wind turbine geometries. (a) 6 m and (b) 4.5 m tower base diameter.

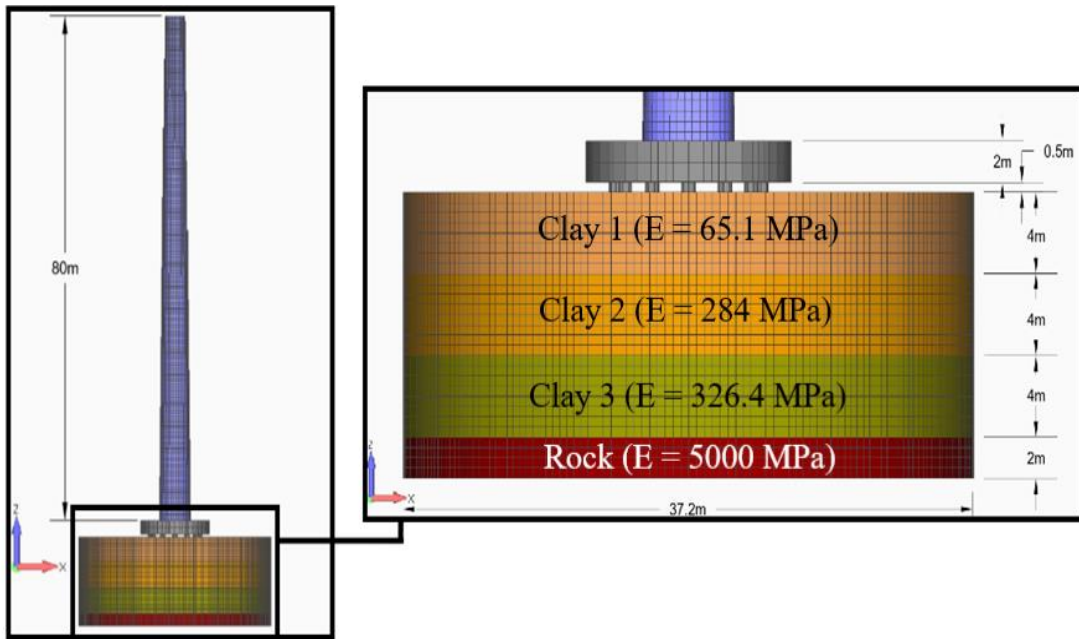
The wind turbine in Fig. 18a was used during the parametric investigation that will be presented in the next section. It is important to note here that the mass of the nacelle, hub and blades were applied at the top of the tower during the analysis as dead loads. Furthermore, the fact that the wind turbine structures are founded on expansive clay led to the selection of a foundation design that foresaw the pile cap being elevated above the soil surface, as it is going to be presented in section 4.2.

## 4.2 SOIL GEOMETRIES

Following the finalization of the wind turbine superstructure and foundation geometry, the different soil profiles were defined. The first geometry that will be referred to as the Equal Layer Geometry, was refined into a model with piles embedded in a rock layer (Fig. 19) and a model with extra soil underneath the piles (Fig. 20).

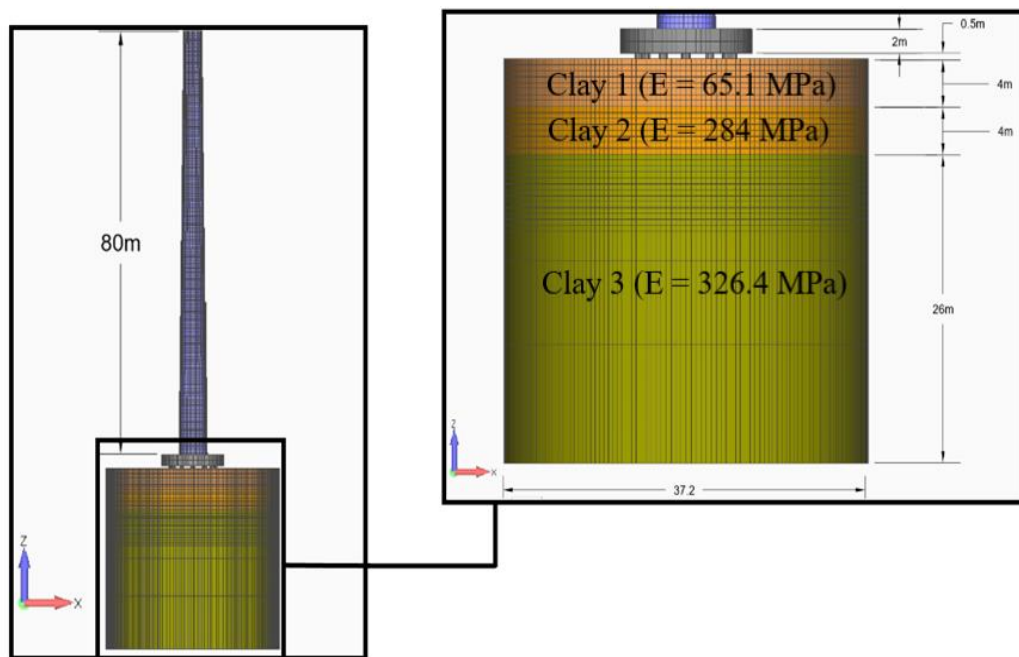
The material properties of the Equal Geometry with the rock layer (EGR) can be seen in Table 2. The soil material properties used within this manuscript were obtained from field tests performed for the needs of the WindAfrica project [9]. The field tests were performed to obtain in-situ results for the clay material at the location of the scheduled SSI experiments that are scheduled to be performed in 2020. Additionally, the material properties of the Equal Geometry model with extra soil can be seen in Table 3. This profile was developed to further investigate the SSI phenomenon for a hypothetical scenario where the clay material was 26 m deep.

The Equal Layer Geometry was then subdivided into soil geometries that contained different pile inclinations. The inclinations were investigated to determine the optimal foundation design of the wind turbine foundation that would derive reduced horizontal displacements during a horizontal loading scenario, where the SFSI effect would be minimized. The inclinations considered were the original geometry (0 degrees from the vertical), 5, 10 and 15 degrees from the vertical axis of the tower. The use of higher inclinations is assumed to be non-practical given the challenges during construction, thus were not included in this investigation. In addition, the findings indicate that higher inclination angles would not lead to improved performances. The exact placement of the 10-degree inclined piles for the Equal Geometry with a rock layer can be seen in Fig. 21, while the geometry of the 10-degree inclined piles for the Equal Layer Geometry with extra soil can be seen in Fig. 22.



1  
2

Figure 19 Equal Layer Geometry with vertical piles embedded in rock.



3  
4  
5

Figure 20 Equal Layer Geometry with vertical piles embedded in extra soil.

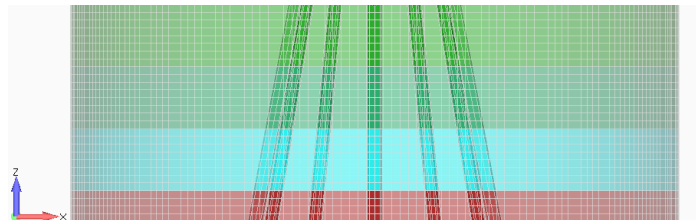
Table 2 Material properties of the Equal Layer Geometry with a rock layer.

Description	Parameters			
	E-value (MPa)	Poisson	Weight (kN/m <sup>3</sup> )	Compressive Strength (kPa)
1 <sup>st</sup> layer (0-4 m)	65.1	0.25	18	36
2 <sup>nd</sup> layer (4-8 m)	284	0.25	18	108
3 <sup>rd</sup> layer (8-12 m)	326.4	0.25	18	180
4 <sup>th</sup> layer (12-14 m)	5,000	0.3	24	30,000
Concrete	20,000	0.3	25	30,000
Steel	210,000	0.3	79	450,000

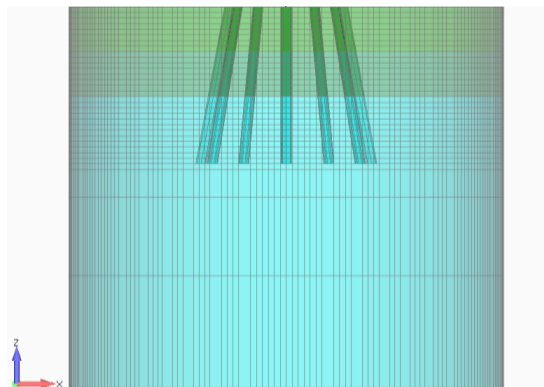
1 Table 3 Material properties of the Equal Layer Geometry with extra soil.

Description	Parameters			
	E-value (MPa)	Poison Ratio	Nominal Weight ( $\text{kN/m}^3$ )	Compressive Strength (kPa)
1 <sup>st</sup> layer (0-4 m)	65.1	0.25	18	36
2 <sup>nd</sup> layer (4-8 m)	284	0.25	18	108
3 <sup>rd</sup> layer (8-26 m)	326.4	0.25	18	248
Concrete	20,000	0.3	25	30,000
Steel	210,000	0.3	79	450,000

2 The second soil geometry constructed herein will be referred to as the Increasing Layer  
 3 Geometry. This geometry was also refined into a model with piles embedded in a rock layer  
 4 (Fig. 23) and a model with extra soil underneath the piles (Fig. 24). This group of profiles was  
 5 developed to further investigate the effect on the numerical response of the structures when  
 6 different soil profiles are assumed. The material properties of the Increasing Layer Geometry  
 7 soil profile with the rock layer can be seen in Table 4, whereas the material properties of the  
 8 Increasing Layer Geometry soil profile with extra soil can be seen in Table 5. The Increasing  
 9 Layer Geometry was also used to construct models that assumed different pile inclinations as  
 10 previously describe.



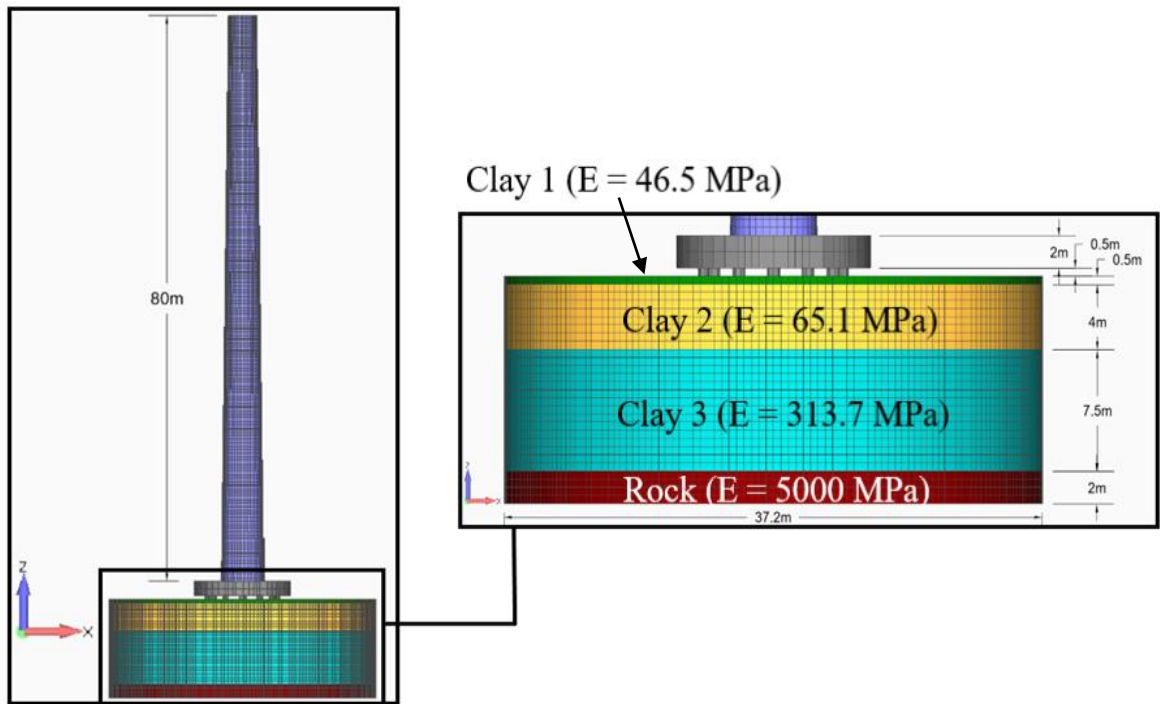
11  
 12 Figure 21 Pile layout of the Equal Geometry with a rock layer with 10-degree pile inclination.



13  
 14 Figure 22 Pile layout of the Equal Geometry with extra soil with 10-degree pile inclination.

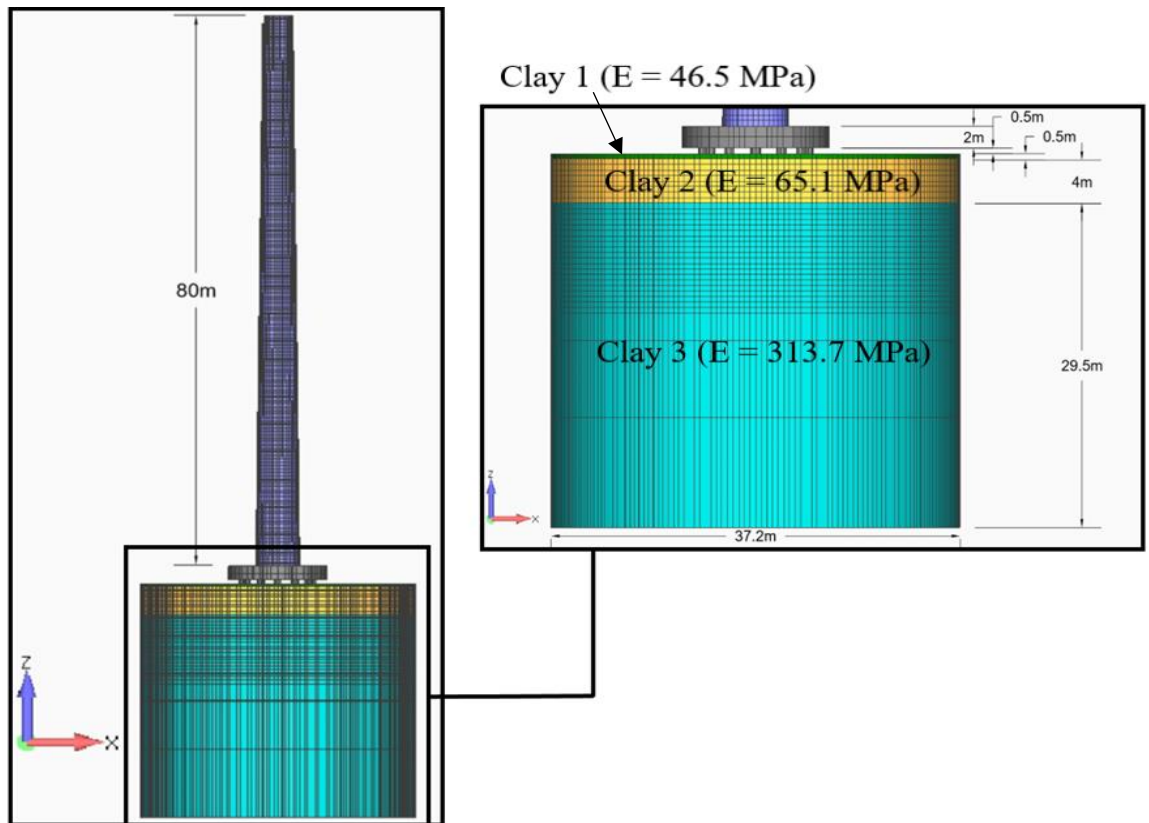
15 The cylindrical soil domains were assumed to be fixed at their base, while the nodes found  
 16 at the perimeter were only allowed to settle along the z-global axis. During the construction of  
 17 the models, local buckling effects were also considered, where the maximum load and stresses  
 18 were determined by using the Euler buckling equations. According to an initial pushover  
 19 analysis, it was found that local buckling would occur at point A that is shown in Fig. 27. The  
 20 local buckling was accounted for by reducing the yielding stress of steel according to Eqs. 16-  
 21 19 in the areas that are expected to develop compression. This approach was adopted to  
 22 minimize the numerical instabilities that would occur during the nonlinear analysis of these  
 23 large-scale models, therefore, avoid the direct modeling of two different types of nonlinearity.

- 1 As it can be seen in Tables 6 and 7, the developed models foresee the use of an average 150,000
- 2 hexahedral elements each, which constitutes computationally demanding numerical models.



- 3
- 4

Figure 23 Increasing Layer Geometry with the piles embedded in a rock layer.



- 5
- 6

Figure 24 Increasing Layer Geometry with the piles embedded in extra soil.

1 Table 4 Material properties of the Increasing Layer Geometry with a rock layer.

Description	Parameters			
	E-value (MPa)	Poison Ratio	Nominal Weight (kN/m <sup>3</sup> )	Compressive Strength (kPa)
1 <sup>st</sup> layer (0.5m)	46.5	0.25	18	20
2 <sup>nd</sup> layer (4m)	65.1	0.25	18	45
3 <sup>rd</sup> layer (7.5m)	313.7	0.25	18	162
4 <sup>th</sup> layer (2m)	5,000	0.3	24	30,000
Concrete	20,000	0.3	25	30,000
Steel	210,000	0.3	79	450,000

2 Table 5 Material properties of the Increasing Layer Geometry with extra soil.

Description	Parameters			
	E-value (MPa)	Poison Ratio	Nominal Weight (kN/m <sup>3</sup> )	Compressive Strength (kPa)
1 <sup>st</sup> layer (0.5m)	46.5	0.25	18	20
2 <sup>nd</sup> layer (4m)	65.1	0.25	18	45
3 <sup>rd</sup> layer (29.5m)	313.7	0.25	18	351
Concrete	20,000	0.3	25	30,000
Steel	210,000	0.3	79	450,000

3  
4 Table 6 Number of elements for the Equal Layer and Increasing Layer Geometry with piles embedded  
5 in rock.

Pile inclination (Degrees)	Number of hexahedral elements - model with piles embedded in rock				RAM requirement for the Stiffness Matrix (Gb)
	Soil	Foundation	Tower	Total	
0	112,728	5,788	6,042	124,558	23
5	123,144	5,788	6,042	134,974	27
10	126,168	5,788	6,042	137,998	28
15	136,584	5,766	6,042	148,392	32

6 Table 7 Number of elements for the Equal Layer and Increasing Layer Geometry with piles  
7 embedded in extra soil.

Pile inclination (Degrees)	Number of hexahedral elements - model with piles embedded in extra soil				RAM requirement for the Stiffness Matrix (Gb)
	Soil	Foundation	Tower	Total	
0	129,408	5,788	6,042	141,238	29
5	141,312	5,788	6,042	153,142	34
10	144,768	5,788	6,042	156,598	36
15	156,672	5,766	6,042	168,480	40

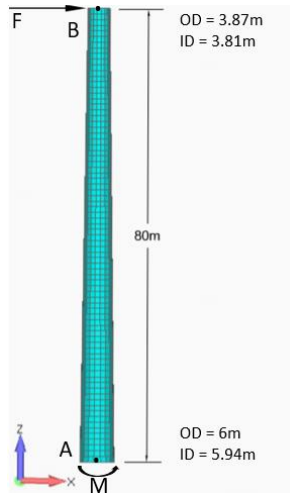


Figure 25 Buckling considerations of the tower.

The moment of inertia at A was determined through the following expression:

$$I_A = \frac{\pi x R^4}{4} \quad (16)$$

$$I_A = 2.51 \text{ m}^4$$

The critical vertical load was then computed by using the Euler buckling equation:

$$P_{cr} = \frac{\pi^2 EI}{KL^2} \quad (17)$$

$$P_{cr} = 122.4 \text{ MN}$$

The critical buckling stress can be calculated as:

$$\sigma = \frac{F}{A} \quad (18)$$

$$\sigma = 217 \text{ MPa}$$

The critical applied horizontal force can be determined:

$$\sigma = \frac{My}{I} \quad (19)$$

where  $M = 80 \text{ m} \times (F)$ , therefore,

$$F = 2.27 \text{ MN}$$

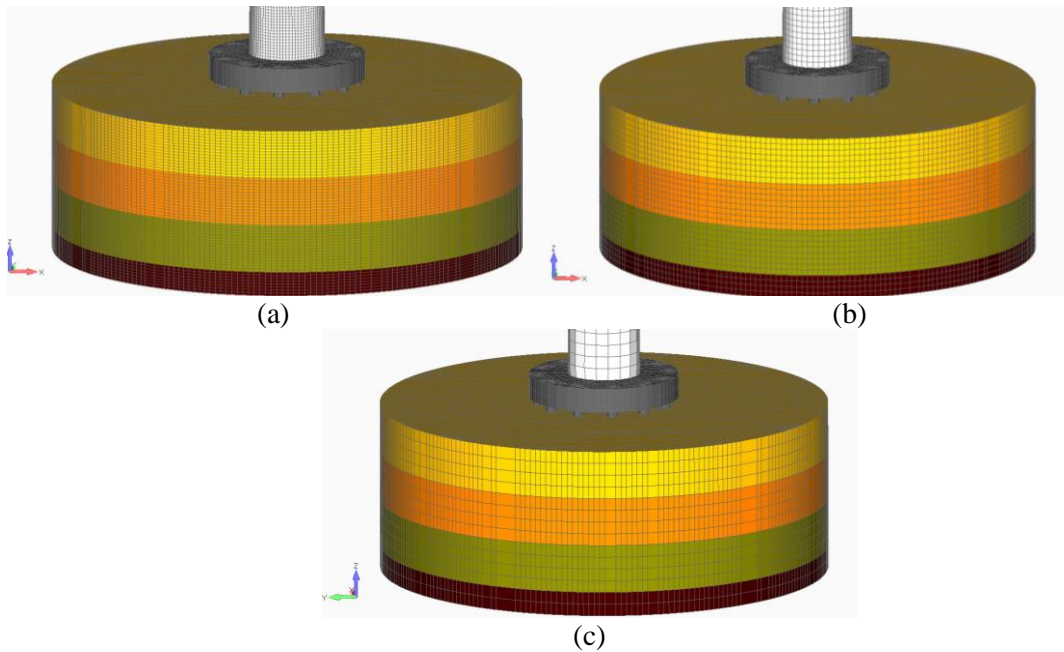
As it was discussed above, in order to avoid performing a nonlinear analysis that will numerically account for two nonlinearity types (material and geometrical) the yielding stress of the steel tower was decreased to 217 MPa in the areas of the steel tower that are expected to develop compression. Thus, avoiding the use of the geometrical nonlinearities during these large-scale analyses. It must be noted here that, the unreduced yielding stress of the tower was set to be equal to 450 MPa.

It is also noteworthy to note here that, an investigation was performed on whether second order effects should be considered during the nonlinear analysis. By considering second order effects, the increase in moment at point A was found to be a mere 2%. The increase in the moment at the base was deemed to be insignificant as the difference compared to the moment derived without second order effects was below 10%. Finally, the force applied at the top of the tower was set to 3 MN to assure that the tower will reach its maximum capacity for all the developed models.

1 **4.3 MESH SENSITIVITY**

2 A mesh sensitivity analysis was performed to determine the optimal FE size to generate the  
 3 most accurate results in a computationally efficient manner. The mesh sizes used in this  
 4 investigation were 0.25 m, 0.5 m and 1 m hexahedral elements (Fig. 26).

5 The frequencies of the first six modes were compared as they resulted from the three models.  
 6 The difference in terms of magnitude between the 0.25 m and the 0.5 m mesh frequencies were  
 7 on average 9.90 % and the difference between the 0.5 m and the 1 m mesh frequencies were  
 8 on average 8.20 %. According to these numerical results, a final decision was made to use 0.5  
 9 m hexahedral elements for both soil and structure in order to achieve an acceptable accuracy  
 10 and avoid the construction of models that will not allow performing this numerical  
 11 investigation due to excessively high computational demand.



12  
13  
14  
15  
16  
17  
18  
19  
20  
21  
22  
23  
24  
25  
26  
27  
Figure 26 Mesh sensitivity models. (a) 0.25 m, (b) 0.5 m and (c) 1 m hexahedral finite element size.

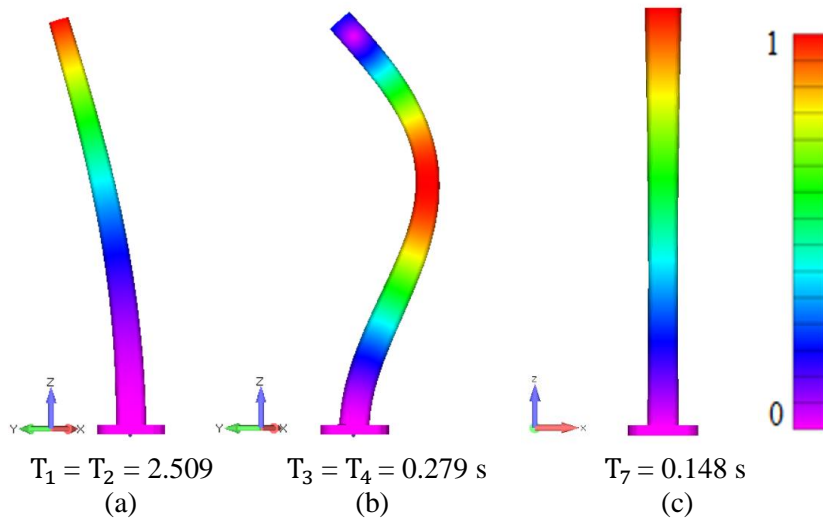
A sensitivity analysis was also performed on different diameters of soil domains by using the model shown in Fig. 26b in order to investigate the effect that the size of the assumed soil mesh size in combination with the adopted boundary conditions have on the numerically obtained frequencies. The original soil profile of 37.2 m in diameter was increased to 55 m, which represents a 32.4% enlargement of the original model. The first 3 eigenfrequencies were numerically estimated and compared in Table 8. It is evident that the largest obtained difference between the two models of 0.13% indicates that the assumed boundary conditions and soil mesh geometry do not affect the derived numerical results.

Table 8 Boundary condition mesh sensitivity results.

Diameter of soil domain	Computed Eigenfrequency		
	1 <sup>st</sup>	2 <sup>nd</sup>	3 <sup>rd</sup>
55 m	0.3757 Hz	0.3758 Hz	3.1913 Hz
37.2 m	0.3757 Hz	0.3758 Hz	3.1871 Hz
<b>Difference between the two models [%]</b>	0%	0%	0.13%

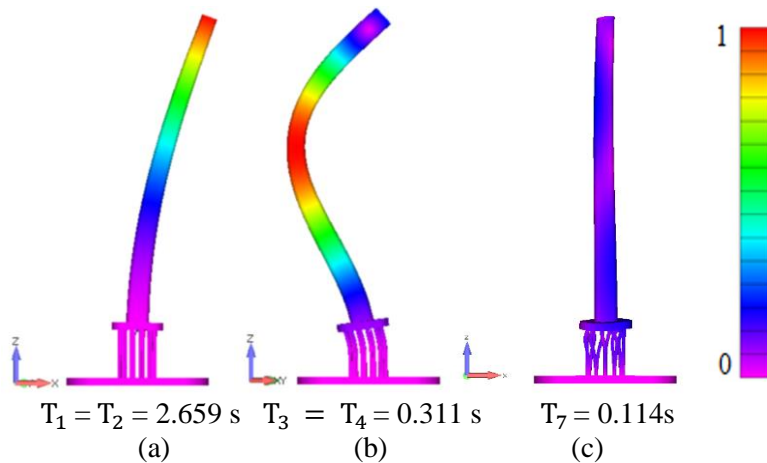
1 **5 MODAL ANALYSIS RESULTS**

2 The modal analyses were performed for the first 24 modes, however, only the first three  
 3 eigenmodes will be discussed for brevity reasons. The deformed shapes and the  
 4 eigenfrequencies will be presented herein as they resulted from the numerical analysis. For  
 5 comparative purposes, a model that foresaw a fixed base (RC pile cap) was constructed and  
 6 analysed. Fig. 27 shows the fixed model (no SSI considerations) and its three modal  
 7 deformation shapes as they were obtained from the numerical model. As it is given in Fig. 27,  
 8 the first two translational modes had a 2.509 seconds period, while the third mode foresaw a  
 9 sinusoidal type of deformation of the tower ( $T_3 = T_4 = 0.279$  s).



10  
11  
12  
13  
14

Figure 27 Deformed shapes of the first three eigenmodes with a fixed condition at the bottom of the pile cap. (a) 1<sup>st</sup> and 2<sup>nd</sup>, (b) 3<sup>rd</sup> and 4<sup>th</sup>, and (c) 7<sup>th</sup> Mode.



15  
16  
17  
18  
19

Figure 28 Deformed shapes of five eigenmodes with a pile inclination of 0 degrees embedded in a rock layer. (a) 1<sup>st</sup> and 2<sup>nd</sup>, (b) 3<sup>rd</sup> and 4<sup>th</sup> and (c) 7<sup>th</sup> Mode.

20 The eigenmodes of the Equal Geometry with a rock layer model and different pile  
 21 inclinations can be seen in Figs. 28-29. The overall results indicated that the first three  
 22 eigenmodes foresee the bending of the steel tower in all cases. It is easy to observe that the  
 23 shape of the modes remained the same compared to the modes shown in Fig. 29, while the  
 24 period duration increased due to the SSI effect. It must be noted here that, the 5- and 15-  
 25 degrees models are not shown due to the similar derived modal shapes. In addition, the last modal shape

1 shown in Figs. 28-31 represent the first mode that foresees a torsional deformation of the  
 2 superstructure.

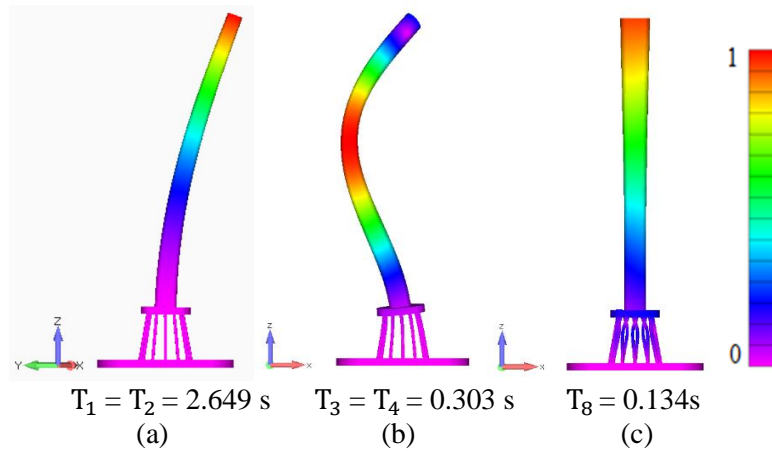


Figure 29 Deformed shapes of the first three eigenmodes with a pile inclination of 10 degrees embedded in a rock layer. (a) 1<sup>st</sup> and 2<sup>nd</sup>, (b) 3<sup>rd</sup> and 4<sup>th</sup>, (c) 8<sup>th</sup> Mode.

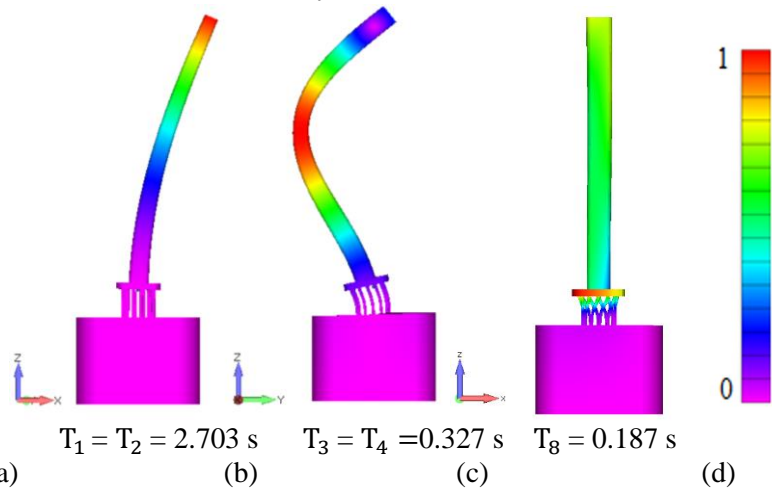


Figure 30 Deformed shapes of the first three eigenmodes with a pile inclination of 0 degrees situated on extra soil. (a) 1<sup>st</sup> and 2<sup>nd</sup>, (b) 3<sup>rd</sup> and 4<sup>th</sup> and (c) 8<sup>th</sup> Mode.

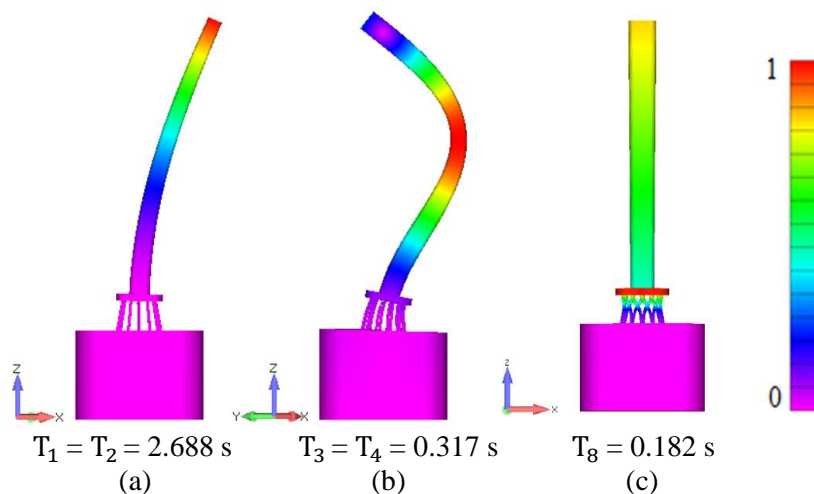


Figure 31 Deformed shapes of the first three eigenmodes with a pile inclination of 10 degrees situated on extra soil. (a) 1<sup>st</sup> and 2<sup>nd</sup>, (b) 3<sup>rd</sup> and 4<sup>th</sup>, (c) 8<sup>th</sup> Mode.

1 Similarly, the first three eigenmodes of the Equal Geometry with extra soil model and  
 2 different pile inclinations can be seen in Figs. 30-31. The Increasing Layer Geometry was also  
 3 studied and the periods that were obtained were used to investigate the difference in results  
 4 when different layer geometries are present. The derived periods for the Equal and Increasing  
 5 Layer Geometry models (with a rock and extra soil) can be seen in Table 9.

6 As it derived from the modal values presented in Table 10 where the comparison between  
 7 the various modal results is given for the case of the Increasing Layer Geometry models, the  
 8 largest difference was obtained during the numerical analysis of the Increasing Layer Geometry  
 9 with the extra soil model with vertical piles, where the period increase was found to be 18.2%  
 10 (Table 10) higher than for the case of mode 3 of the fixed model. This phenomenon is attributed  
 11 to the SSI effect that maximizes when the piles are not embedded within the layer of rock,  
 12 deriving a more flexible behaviour. When the piles are embedded in clay throughout their  
 13 height and never reach the healthy bedrock, the foundation becomes more flexible due to its  
 14 ability to deform and develop larger settlement and rotations, where the computed  
 15 eigenfrequencies are found to be lower. Similar results derived for the case of the first two  
 16 modes that were predicted from the Increasing Layer Geometry with the extra soil model,  
 17 where the increase was found to be equal to 8%. It is evident that when the piles are founded  
 18 on a bedrock, the foundation system is found to be practically fixed at the tips of the piles,  
 19 where the additional flexibility in this case is controlled by the stiffness of the piles (number  
 20 of piles, length and diameter).

21 Table 9 Modes for the Increasing Layer Geometry models.

Inclination (Degrees)	Rock Layer			Extra Soil		
	Mode (s)					
	1	2	3	1	2	3
<b>0</b>	2.662	2.661	0.313	2.709	2.709	0.330
<b>5</b>	2.651	2.651	0.307	2.697	2.696	0.324
<b>10</b>	2.651	2.651	0.303	2.692	2.692	0.319
<b>15</b>	2.657	2.657	0.302	2.694	2.694	0.316

22 Table 10 Difference in periods of the under-study SSI models and the fixed tower for the Increasing  
 23 Layer Geometry.

Inclination (Degrees)	Extra Soil			Rock		
	Mode difference (%)					
	1	2	3	1	2	3
<b>0</b>	7.97	7.95	<b>18.15</b>	6.06	6.03	<b>12.29</b>
<b>5</b>	7.45	7.46	15.94	5.64	5.65	9.98
<b>10</b>	7.28	7.28	14.33	5.64	5.63	8.66
<b>15</b>	7.35	7.35	13.31	5.88	5.88	8.14

24 Table 11 Difference in periods of the under-study SSI models and the fixed tower for the Equal Layer  
 25 Geometry.

Inclination (Degrees)	Extra Soil			Rock		
	Mode difference (%)					
	1	2	3	1	2	3
<b>0</b>	7.76	7.74	<b>17.07</b>	5.97	5.95	<b>11.66</b>
<b>5</b>	7.28	7.28	15.08	5.58	5.58	9.60
<b>10</b>	7.11	7.11	13.64	5.56	5.56	8.52
<b>15</b>	7.17	7.17	12.73	5.77	5.77	8.04

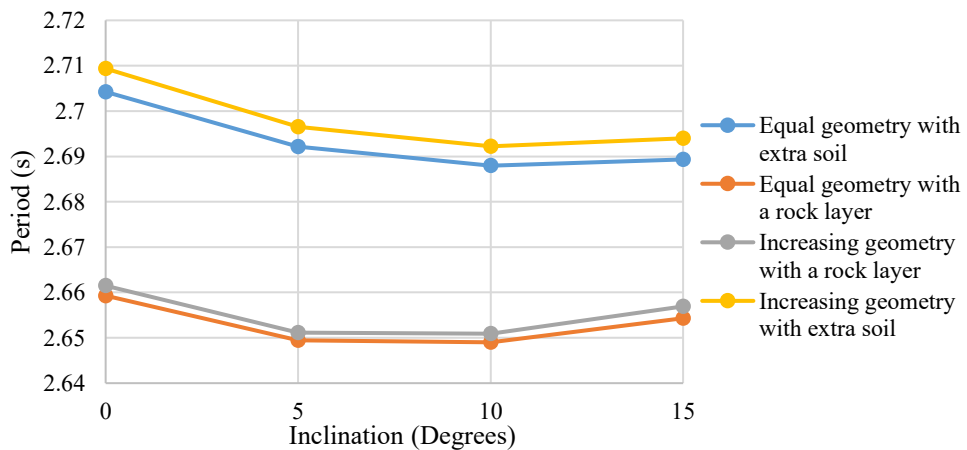
1 Table 11 shows the comparison between the fixed model and the Equal Layer Geometry  
 2 models, where it is easy to observe that the SSI effect is evident. For the case of the model with  
 3 extra soil and vertical piles, a 17.07% increase was noted for the case of the 3<sup>rd</sup> mode, while a  
 4 7.75% average increase for the case of the first two modes was computed. It is also evident that  
 5 the difference in terms of mode duration decreases as the pile inclination increases up to a 10  
 6 degrees angle, where the mode duration increases again for a 15 degrees angle.

7 **5.1 FURTHER ANALYSIS OF THE MODAL RESULTS**

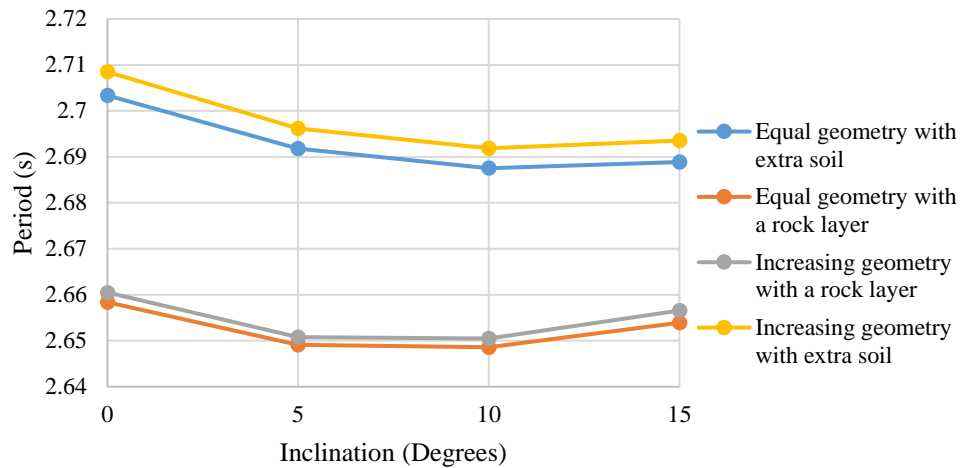
8 The periods of the different soil geometries and foundation configurations were compared  
 9 for the 1<sup>st</sup>, 2<sup>nd</sup> and 3<sup>rd</sup> eigenmodes. All the corresponding eigenmodes of the different models  
 10 were found to derive similar modal shapes. As it was mentioned above, the first two  
 11 eigenmodes foresaw a translational oscillation along the x and y global directions, as the wind  
 12 turbine is doubly symmetric. Moreover, the 3<sup>rd</sup> eigenmode of all geometries provided a double  
 13 curvature deformation and a contribution from the RC piles through a relative bending-like  
 14 deformation.

15 To further compare the obtained results, Fig 32 was developed based on the modal analysis  
 16 and Table 8, where the different predicted modal values are shown. As it can be seen, the  
 17 geometry with the rock layer yielded a stiffer behaviour than that of the extra soil for all the  
 18 models that were analysed herein. However, for both soil profile scenarios the pile inclination  
 19 of 10 degrees provided a lower period, indicating a stiffer behaviour compared to the rest  
 20 foundation geometries. These results were attributed to the optimal pile inclination, as well as,  
 21 more stiffness provided by the inclined piles of 10 degrees. Further investigation can provide  
 22 the exact inclination, even though this will not be of practical interest if we consider that we  
 23 are dealing with a RC foundation that assumes 14 m long piles, thus, constructing inclinations  
 24 with an accuracy close to 1° is not easy to achieve when constructing this size of foundations.

25 The Equal Geometry and the Increasing Layer Geometry derived similar eigenmode values  
 26 during this numerical investigation, however, it is evident that the soil geometry has an  
 27 influence on the stiffness of the Wind Turbine structure. Nevertheless, the difference in terms  
 28 of period values is not of practical interest, whereas these differences can be seen in Figs. 32,  
 29 33 and 34, where the modal values of the first three modes are graphically illustrated.  
 30

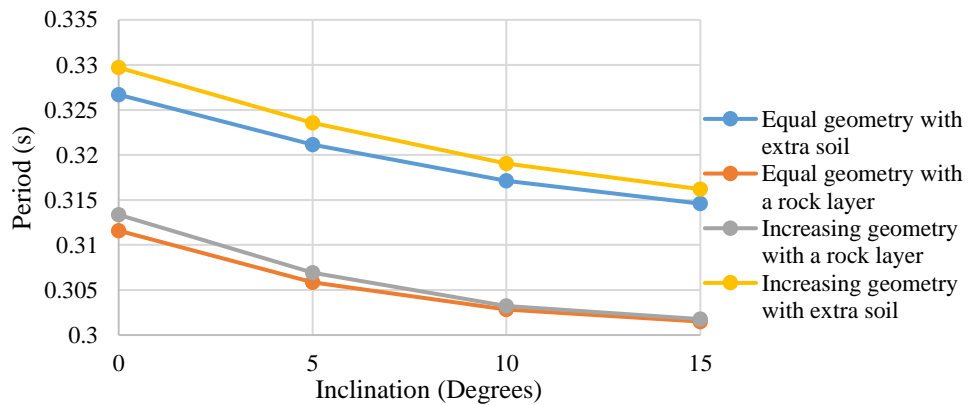


31 Figure 32 Period comparison of the rock layer and extra soil results for the 1<sup>st</sup> eigenmode.  
 32



1  
2

Figure 33 Period comparison of the rock layer and extra soil results for the 2<sup>nd</sup> eigenmode.



3  
4

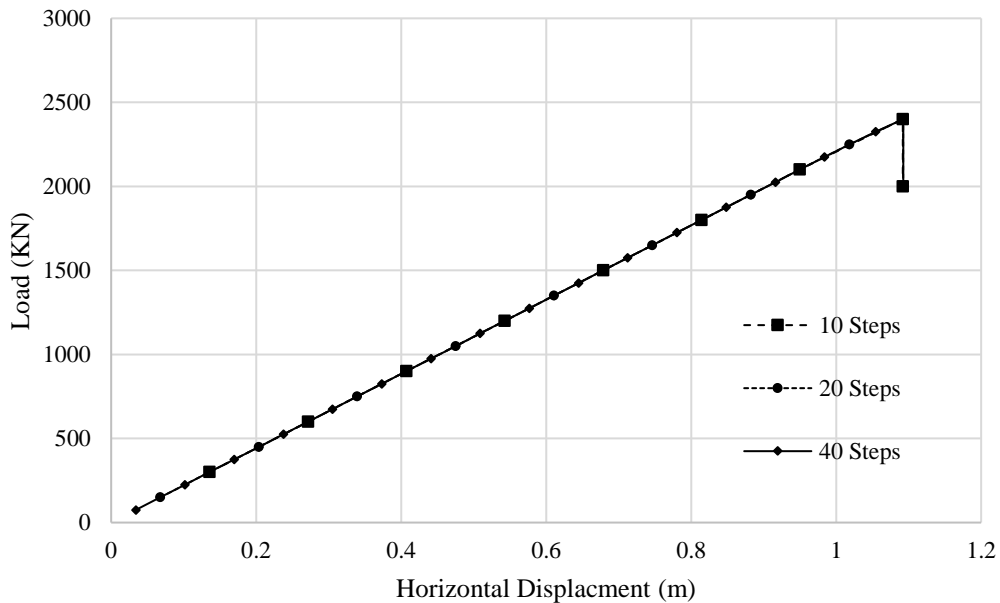
Figure 34 Period comparison of the rock layer and extra soil results for the 3<sup>rd</sup> eigenmode.

5 As it can also be seen in Figs. 32 and 33 the rock layer geometries had the lowest periods  
 6 due to the hard rock that provides a stiff base to the pile foundation. The numerical investigation  
 7 of the 3<sup>rd</sup> eigenmode yielded a minimum period value for the 15-degree pile inclination (see  
 8 Fig. 34), which is attributed to the shape of this mode that foresees a higher contribution of the  
 9 piles through their respective bending. Due to the larger pile inclination, the piles are found to  
 10 require larger energy to bend thus the 3<sup>rd</sup> mode is found to exhibit a lower period duration. As  
 11 it was mentioned above, the modes of interest are the first two, which foresee the deformation  
 12 along the x and y global axes, therefore, based on the obtained results these are the modes that  
 13 will contribute the most when a horizontal load is applied on the structure. Conclusively, the  
 14 10 degrees piles are found to derive the optimum performance out of all the foundation  
 15 geometries that were investigated in this work, hence, this is the foundation that will be used  
 16 during the pushover analysis investigation.

## 17 5.2 INVESTIGATION OF THE PUSHOVER STEP SIZE

18 Prior to performing the pushover analysis investigation, a parametric study was performed  
 19 on the load step size given that the large-scale models require a significant computational time  
 20 to be solved in a nonlinear manner for multiple steps. Therefore, the minimization of the  
 21 required load steps is needed to be performed at this stage, thus select the optimum numerical  
 22 strategy during the pushover analysis.

1 For this reason, the model without SSI considerations (fixed at the base of the pile cap) was  
 2 subjected to a nonlinear analysis with different step size increments. The step increment was  
 3 also investigated to verify the numerical robustness and objectivity of the nonlinear solution  
 4 algorithm when different load increments are assumed. For the needs of this investigation, three  
 5 analyses were performed by assuming 10, 20 and 40 load steps. It is evident in Fig. 35 that all  
 6 analyses failed for a total applied load of 2400 kN, where the steel tower was found to develop  
 7 local buckling at the base. Considering the computational demand of the SSI models and the  
 8 required accuracy, it was decided to use 20 incremental steps in all pushover analyses.



9

10

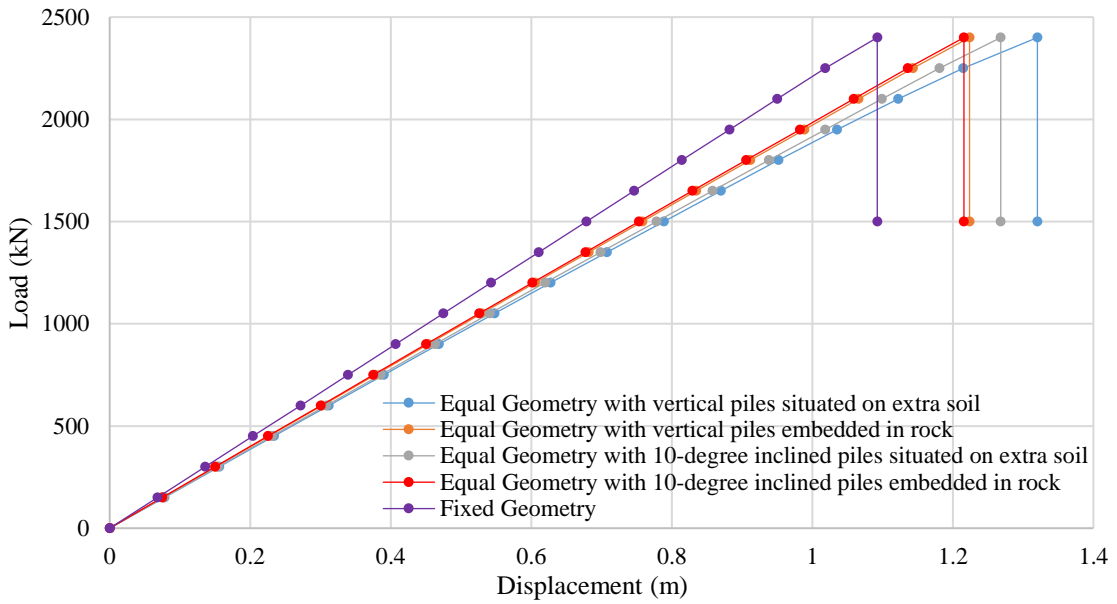
Figure 35 Load vs Horizontal Displacement. Step-size investigation.

## 11 6 PUSHOVER ANALYSES RESULTS

12 The pushover analyses were conducted by applying a horizontal force of 3 MN, where all  
 13 dead loads were accounted for. The vertical and 10-degree inclination piles of the Equal and  
 14 Increasing Layer Geometry models were analysed. The P- $\delta$  curves for the various models were  
 15 compared, where the Applied Load vs Pile Cap Rotation was also investigated.

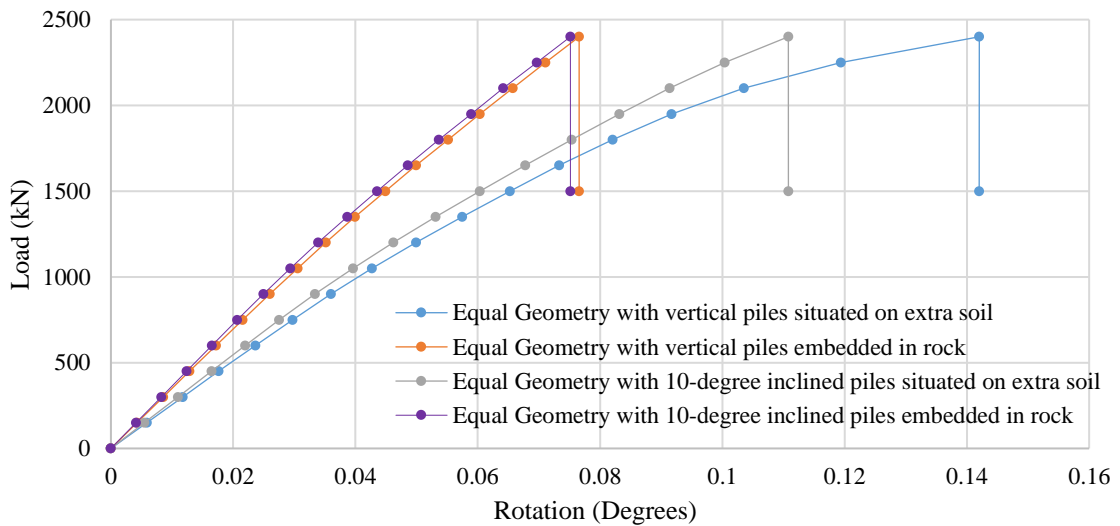
### 16 6.1 EQUAL LAYER GEOMETRY MODELS

17 The P- $\delta$  curves of the Equal Layer Geometry models can be seen in Fig. 36. It must be noted  
 18 here that all the models derived a failure due to local buckling at the base of the steel tower,  
 19 but for a different total horizontal deformation. This is attributed to the SFSI effect of all the  
 20 different soil geometries that result different foundation flexibility, thus affect the overall  
 21 lateral displacement prior to failure. Therefore, according to the numerical findings, each soil  
 22 profile affects the overall foundation rotation, where the corresponding superstructure  
 23 deformation was also affected, developing lateral displacements and strain concentrations that  
 24 were controlled from the foundation settlement and rotation. According to the obtained  
 25 numerical results, the Equal Layer Geometry with 10-degree inclined piles embedded in rock  
 26 yielded the smallest displacement prior to failure. A mechanical behaviour attributed to the  
 27 stiffness increase due to the rock layer combined with the pile inclination.



1  
2

Figure 36 P- $\delta$  curves of the Equal Layer Geometry models.



3  
4

Figure 37 Rotation of the pile cap for the Equal Layer Geometry models.

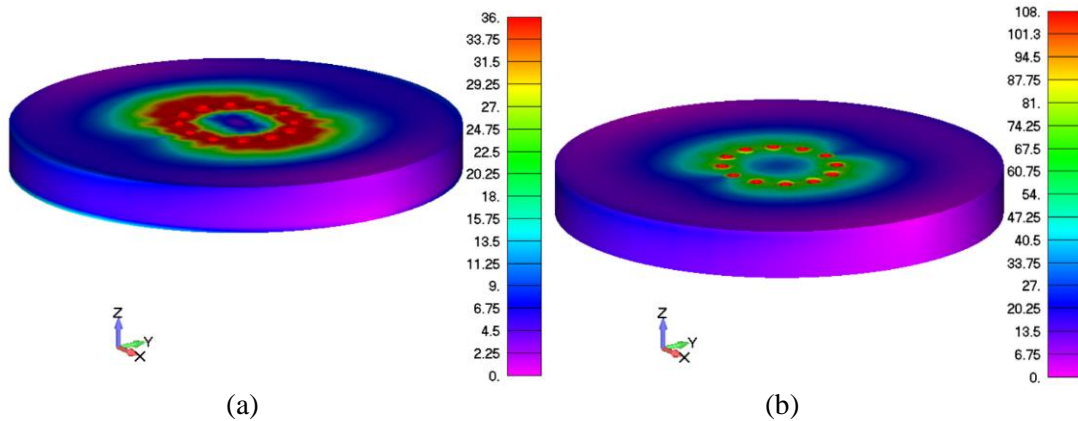
5 The significance of SFSI can yet again be observed when comparing the displacement at  
 6 failure of the SSI models and the fixed model (Fig. 36). According to the numerical findings,  
 7 the SSI derived a total of 26.8% increase in terms of horizontal displacement prior to failure  
 8 for the case of the model with vertical piles founded on soft extra soil. This numerical finding  
 9 is attributed to the ability of the foundation to deform and rotate given the flexibility of the soil  
 10 that surrounds the vertical piles.

11 The rotation of the RC pile cap for the under-study models can be seen in Fig. 37. As  
 12 expected, the foundation where the piles are situated on extra soil yielded a larger rotation than  
 13 the models that assumed to be founded on a rock layer. The Equal Layer Geometry with 10-  
 14 degree inclined piles embedded in rock exhibited the lowest rotation out of the four models  
 15 that were investigated (foundation and soil profiles), illustrating the improved mechanical  
 16 response of the foundation when the piles are inclined. According to the numerical predictions,  
 17 when a 10-degree inclination is adopted the pile cap rotation is decreased by 22% prior to  
 18 failure, a finding that highlights the improved behavior of the foundation system. Based on the

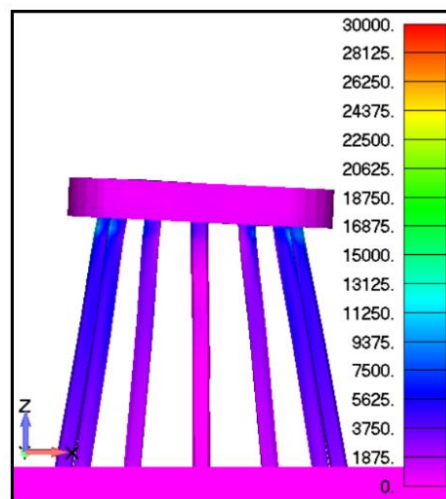
1 shape of the numerically obtained curves, it is easy to conclude that the soil developed plastic  
 2 regions, thus entered the nonlinear state (see Fig. 37 cases with extra soil). It is also easy to  
 3 conclude that the model with battered piles minimizes these nonlinearities, exhibiting an  
 4 improved mechanical response.

5 The nonlinear increase in rotation of the pile cap for the Equal Geometry with vertical piles  
 6 situated on extra soil (Fig. 37) is due to the yielding of the soil that occurred during the  
 7 nonlinear analysis. The stress exceedance can be observed in Fig. 38, where the soil in the 1<sup>st</sup>  
 8 layer around the piles yielded at 36 kPa (Fig. 38a). The Equal Geometry model with 10-degree  
 9 inclined piles situated on extra soil had the same behaviour as previously discussed, but the  
 10 observed level of plastification was less than that of the vertical piles.

11 The deformed shape of the pile cap for the optimum foundation design can be seen in Fig.  
 12 39, where the von Mises stress distribution is given. As it can be observed, the maximum  
 13 developed stresses were found to develop at the piles' heads where the pile cap is connected to  
 14 the RC piles. It is evident that the stresses that develop at the base of the steel tower are  
 15 transferred trough these connections to the RC piles, where the loads are thereafter transferred  
 16 to the soil domain, stressing those connection areas that develop concentrated strains.



17  
 18  
 19  
 20 Figure 38 Solid von Mises stress prior to failure of the Equal Layer Geometry with vertical piles embedded in extra soil (kPa). (a) 1<sup>st</sup> layer and (b) 2<sup>nd</sup> layer.



21  
 22  
 23 Figure 39 Deformed shape prior to failure of the pile cap of 10-degree inclined piles embedded in rock (Deformation scale x20, stress in kPa).

24 In addition to the above, the overall SFSI effect can be further quantified when comparing  
 25 the displacement at failure of the SSI and the fixed models (see Table 12). The 10-degree

1 inclined pile geometry with extra soil had the highest displacement increase (16.51%),  
 2 compared to the 10-degree inclined pile model founded on bedrock that restrained the  
 3 corresponding displacement increase to 10.6% compared to the fixed model. This mechanical  
 4 response was expected given the stiffness that is induced to the system when the bedrock layer  
 5 is assumed.

6 Table 12 Difference between the 10-degree inclined pile Equal Layer Geometry and the Fixed  
 7 Geometry.

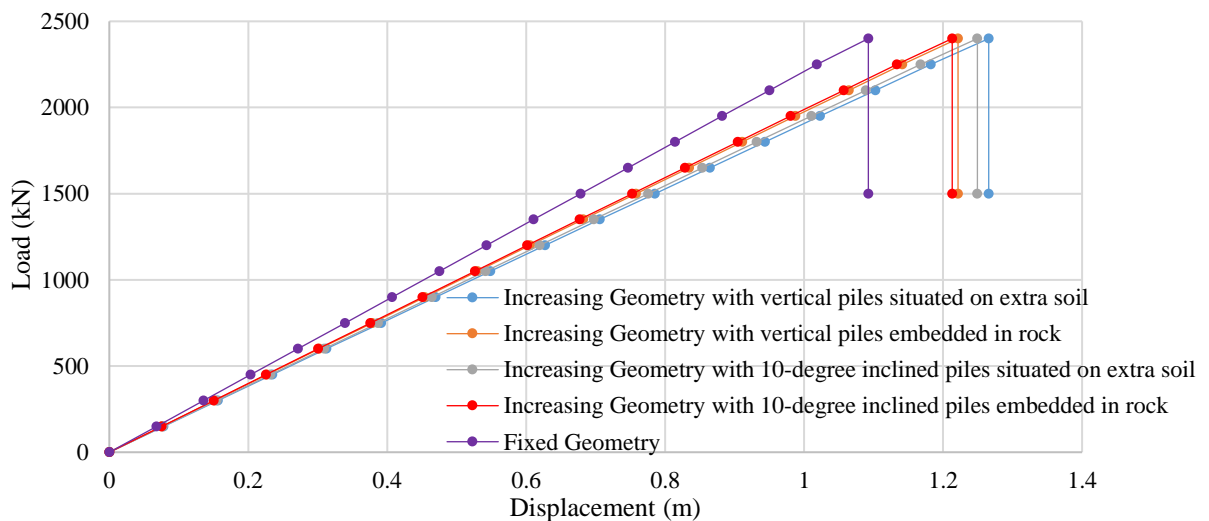
Model	Displacement increase
Extra soil	16.51 %
Rock	10.58 %

8 **6.2 INCREASING LAYER GEOMETRY MODELS**

9 The SFSI effect for the case of the models that foresaw the use of the Increasing Layer  
 10 Geometry is shown in Table 13, where it is easy to depict that the model founded on soft soil  
 11 derived a 13.31% displacement increase prior to failure when compared to the fixed model.  
 12 This verifies the more flexible behaviour of the SSI models, whereas it is evident that, when  
 13 the second soil profile is adopted a stiffer behaviour derives when compared to the Equal Layer  
 14 Geometry soil profile (see Table 12). This is a clear indication that the soil profile plays a  
 15 significant role in the overall mechanical response of the tower, thus investigations based on  
 16 realistic in-situ conditions have to be performed when dealing with this type of structures and  
 17 foundation systems.

18 Table 13 Difference between the 10-degree inclined pile Increasing Layer Geometry and the Fixed  
 19 Geometry.

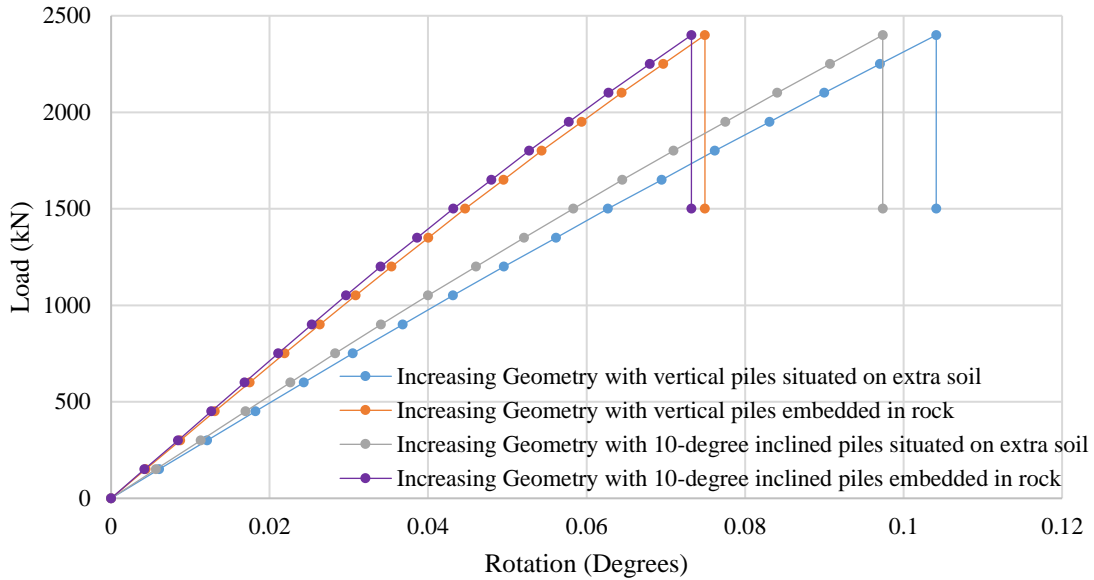
Model	Displacement increase
Extra soil	13.31 %
Rock	10.33 %



20  
 21

Figure 40 P- $\delta$  curves of the Increasing Layer Geometry models.

1 Based on the numerical results, it was found that the 10-degree inclined and vertical piles  
 2 embedded in rock have a smaller difference in terms of displacement at failure (see Fig. 40)  
 3 compared to the previous results that were found to derive a larger SFSI effect. Once more, the  
 4 numerical findings indicate that the 10-degree inclined piles model embedded in rock yielded  
 5 the lowest horizontal displacements.



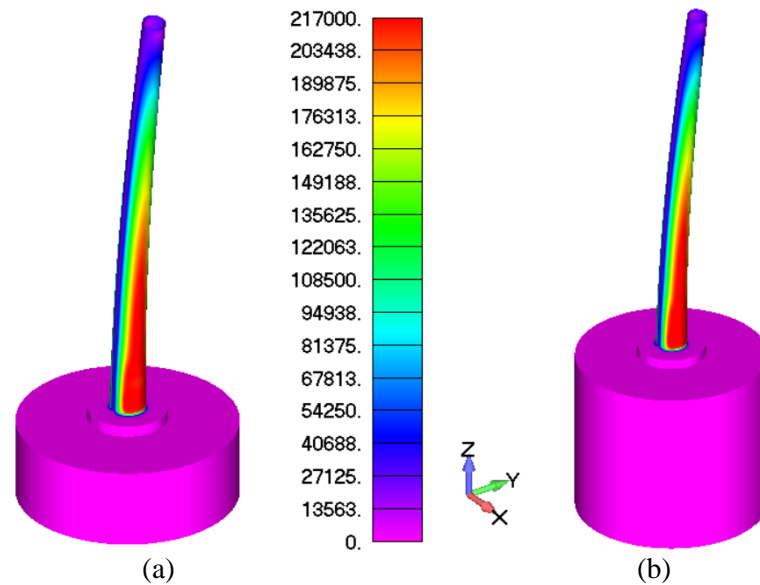
6  
 7 Figure 41 Rotation of the pile cap for the Increasing Layer Geometry models.

8 The corresponding rotation of the pile cap for the under-study Increasing Layer Geometry  
 9 soil profile models can be seen in Fig. 41. The Increasing Layer Geometry with 10-degree  
 10 inclined piles embedded in rock had the lowest rotation out of the investigated increasing layer  
 11 soil profile models, while when comparing the computed rotation for the case of the vertical  
 12 piles it is easy to conclude that the 10-degree pile inclination stiffens the mechanical behaviour  
 13 of the foundation, minimizing the soil nonlinearities during the analysis. Finally, when  
 14 comparing the results obtained in Fig. 37 and Fig. 41, it is easy to observe the more flexible  
 15 behaviour when the Equal Layer Geometry soil profile is used, highlighting the overall effect  
 16 of the SFSI when different soil profiles are assumed. The increase of the pile cap rotation prior  
 17 to failure was computed to be equal to 36.5% for the case of the vertical pile foundation models  
 18 embedded in extra soil. Thus, the Equal Layer Geometry model with vertical piles on extra soil  
 19 was found to be significantly more flexible compared to the Increasing Layer Geometry model  
 20 with vertical piles on extra soil.

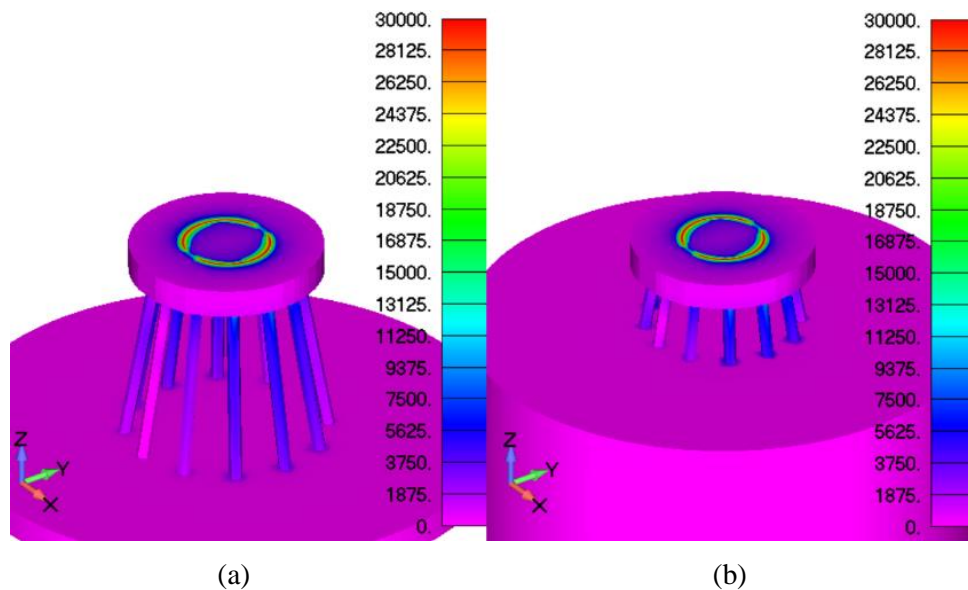
21 **6.3 MECHANICAL RESPONSE OF THE TOWER AND STRESS**  
 22 **DISTRIBUTION**

23 The stress distribution of the 10-degree inclined piles on extra soil and embedded in rock  
 24 are shown in this section for the Increasing Layer Geometry soil profile. Fig. 42 shows the von  
 25 Mises stress prior to failure for the two different soil profile assumptions (with and without a  
 26 rock layer). The figure shows the case of the load increment where the steel tower develops  
 27 local buckling and fails, where it is evident that the stress distribution of the two models is  
 28 similar. The deform shape, was also found to be similar with the overall horizontal deformation  
 29 being 5% larger for the case of the extra soil model.

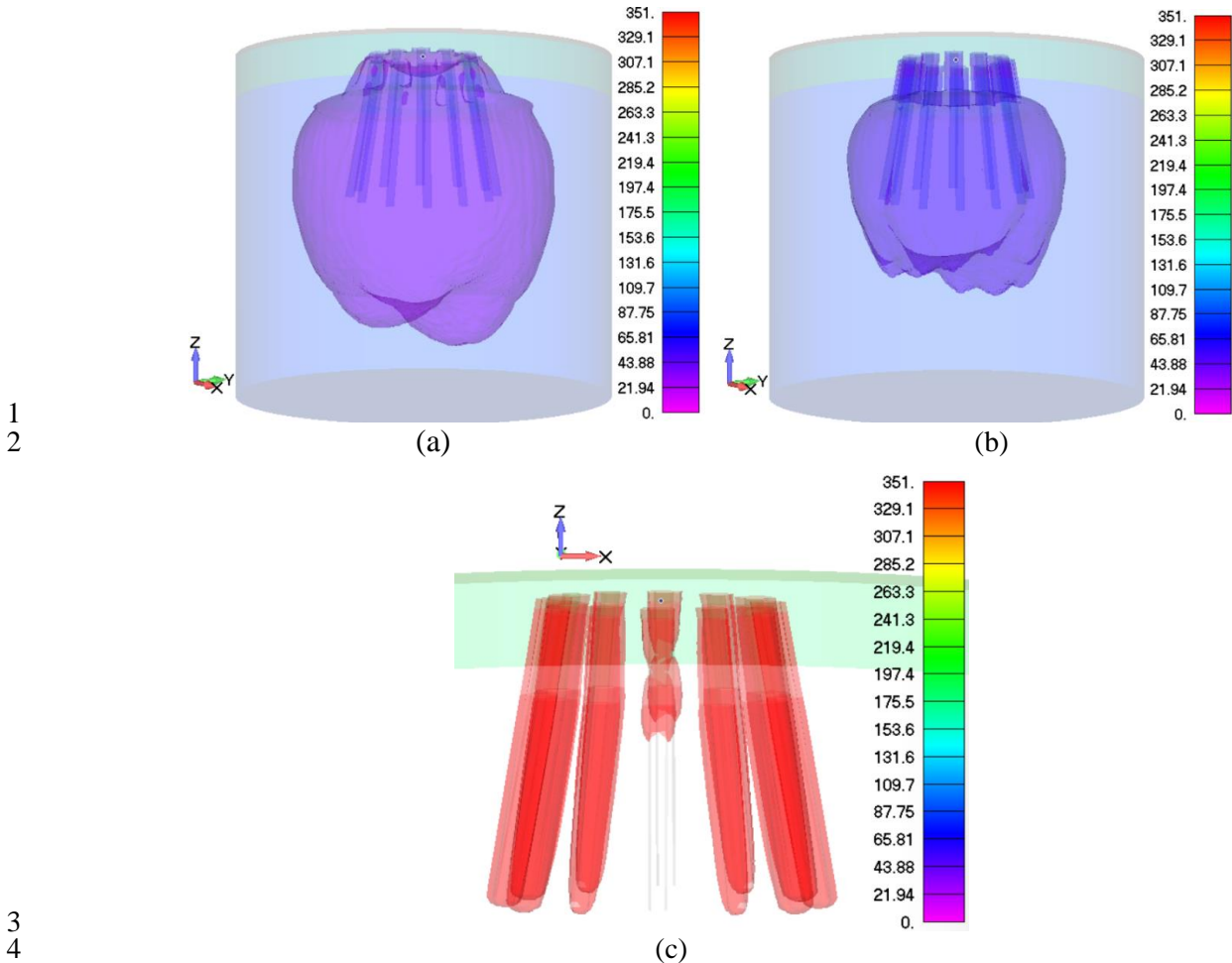
1 Fig. 43 shows the von Mises stress contours of the foundations' RC domain prior to failure.  
 2 The stress concentrations of the tower-concrete interface can be seen in this figure. It can be  
 3 noted that no local failure of the concrete was predicted, where the piles located on the neutral  
 4 axis of the pile cap were found to developed very small stresses. However, larger stresses  
 5 occurred further away from the neutral axis where the RC piles develop larger deformations  
 6 based on the loads applied to the structure. Therefore, it is easy to conclude that the critical  
 7 structural member is the steel tower that caused the wind turbine to fail due to local buckling.  
 8 The dynamic iso-surface stress distribution for the Increasing Layer Geometry with piles  
 9 embedded in extra soil prior to failure can be seen in Fig. 44, for soil stress levels of 20, 45,  
 10 351 kPa.



11  
 12  
 13 Figure 42 Increasing Layer Geometry models. Solid von Mises stress contours for the case of 10-  
 14 degrees inclined piles. Deformed shape of the tower for (a) Piles embedded in a rock layer and (b)  
 15 Piles situated on extra soil (kPa).



16  
 17  
 18 Figure 43 Solid von Mises stress contour. Stress distribution in the concrete foundation prior  
 19 to failure (a) Piles embedded in a rock layer and (b) Piles situated on extra soil (kPa).



1  
2

3  
4  
5  
6

Figure 44 Stress distribution beneath the 10-degree inclined piles situated on extra soil for the Increasing Layer Geometry (a) 20 kPa, (b) 45 kPa and (c) 351 kPa.

7 **7 CONCLUSIONS AND RECOMMENDATIONS**

8 An excessive investigation was performed on the effect of the SFSI phenomenon on wind  
 9 turbine structures using 3D detailed models. The proposed modelling approach foresaw the use  
 10 of hexahedral elements to discretize all the domains of the SSI models, where modal and  
 11 pushover analyses were performed. A pushover validation model with SSI considerations was  
 12 constructed according to the experimental setup found in [10] and was found to derive good  
 13 results in comparison to the experimental data.

14 Thereafter, a numerical investigation on wind turbine structures and their dynamic response  
 15 was performed by assuming an 80 m tall wind turbine tower that was founded on clay soil  
 16 material. Based on the numerically obtained results, all soil profile models revealed that the  
 17 optimum inclination of the piles was that of 10-degrees measured from the vertical. This  
 18 finding is not in line with previous findings that concluded that the angle of the piles should be  
 19 equal or larger than 15 degrees. Given that the research work presented in this manuscript  
 20 foresaw the use of hexahedral elements for discretizing both piles and soil domains, it is easy  
 21 to conclude that the numerical accuracy that was used to derive the numerical results herein is  
 22 higher compared to other existing research work that used the more simplistic beam-column  
 23 finite elements. Therefore, based on the research findings presented in this work, the optimum  
 24 pile angle suggested is that of 10 degrees.

1 After concluding on the optimum inclination angle of the foundation piles, pushover  
2 analyses were performed to further investigated the mechanical response of the optimum  
3 foundation configuration that derived from the modal analyses. Both soil profiles were  
4 investigated under nonlinear loading conditions, where the Increasing Layer Geometry with  
5 10-degree pile inclination situated on extra soil and embedded in rock were found to yield the  
6 lowest pile cap rotations and tower horizontal displacements prior to failure. This numerical  
7 finding highlights the different level that the SFSI affects the overall mechanical behaviour of  
8 the structure for different soil profiles. Therefore, it is strongly recommended to perform a  
9 numerical investigation based on the in-situ soil profile to determine the optimum foundation  
10 design.

11 According to the stress analysis that was performed in this research work, it was found that  
12 the 10-degree piles decreased the stress development within the soil domain compared to the  
13 vertical pile configuration. Therefore, it is safe to conclude that by adopting battered piles the  
14 soil stress levels are decreased significantly minimizing the possibilities of developing  
15 nonlinearities within the soil domain. This research finding is in line with previous research  
16 studies, confirming the mechanical improvement of the wind turbine structures when battered  
17 piles are used.

18 In addition to the above, the numerical investigation verified that it is always preferable to  
19 design wind turbine structures' piles to be embedded in a rock layer, if feasible. This will ensure  
20 not only the safe transfer of the stresses to the bedrock, but it will minimize the deformations  
21 and horizontal displacement of the tower as well. Conclusively, it is essential to thoroughly  
22 investigate the effect of SFSI on the superstructure prior to finalizing and optimally designing  
23 a wind turbine structure's foundation system.

24 As a future step in optimizing the proposed structural design presented in this research work,  
25 a tower redesign is necessary to be performed so as to adjust the steel thicknesses based on the  
26 stress analysis that was performed, minimizing the required material to manufacture the tower.  
27 Furthermore, full-scale nonlinear dynamic analysis will be performed to further investigate the  
28 overall response of the proposed design and parametrically investigate the ability of the  
29 proposed design to minimize stress development at the soil, substructure and superstructure  
30 domains.

## 31 **8 ACKNOWLEDGEMENT**

32 The analysis of the developed large-scale numerical models were performed through the use  
33 of a fast PC that was purchased under the financial support received from the Research  
34 Development Programme (RDP), year 2019, round No 1, University of Pretoria, under the  
35 project titled Future of Reinforced Concrete Analysis (FU.RE.CON.AN.); a research fund  
36 awarded to the second author in support to his research activities. This financial support is  
37 highly acknowledged. The authors would also like to acknowledge S.W. Jacobsz and G.  
38 Heymann, University of Pretoria, for providing with the soil profile experimental data that were  
39 used for the needs of this research work.

## 40 **9 REFERENCES**

- 41 [1] Mourlas, C., Papadrakakis, M. and Markou, G. (2017), "A Computationally Efficient Model  
42 for the Cyclic Behavior of Reinforced Concrete Structural Members", *Engineering Structures*,  
43 141, pp. 97–125.

- 1 [2] Mourlas, C., Markou, G. and Papadrakakis, M. (2019), “Accurate and Computationally  
2 Efficient Nonlinear Static and Dynamic Analysis of Reinforced Concrete Structures  
3 Considering Damage Factors”, *Engineering Structures*, 178 (2019), pp. 258–285.
- 4 [3] Mourlas, C., Markou, G., and Papadrakakis, M., “3D Detailed Modeling of Reinforced  
5 Concrete Frames Considering accumulated damage during static cyclic and dynamic analysis  
6 – new validation case studies”, *COMPdyn 2019, 7th International Conference on  
7 Computational Methods in Structural Dynamics and Earthquake Engineering*, 24-26 June 2019,  
8 Crete, Greece.
- 9 [4] Markou, G., Sabouni, R., Suleiman, F. and El-Chouli, R. (2015), “Full-Scale Modeling of the  
10 Soil-Structure Interaction Problem Through the use of Hybrid Models (HYMOD)”,  
11 *International Journal of Current Engineering and Technology*, 5 (2), pp. 885-892.
- 12 [5] Markou, G., AlHamaydeh, M. and Saadi, D., “Effects of the Soil-Structure-Interaction  
13 Phenomenon on RC Structures with Pile Foundations”, *9th GRACM International Congress on  
14 Computational Mechanics*, Chania, Greece, 4-6 June 2018, pp. 338-345.
- 15 [6] Mourlas, C., Gravett, D.Z., Markou, G., and Papadrakakis, M., “Investigation of the Soil  
16 Structure Interaction Effect on the Dynamic Behavior of Multistorey RC Buildings”, *VIII  
17 International Conference on Computational Methods for Coupled Problems in Science and  
18 Engineering*, *COUPLED PROBLEMS 2019*, 3-5 June 2019, Sitges, Catalonia, Spain.
- 19 [7] Austin, S. and Jerath, S. 2017. “Effect of soil-foundation-structure interaction on the seismic  
20 response of wind turbines”. *Ain Shams Engineering Journal*, Vol 8, May, pp 323-331.
- 21 [8] De Risi, R., Bhattacharya, S. and Goda, K. 2018. “Seismic performance assessment of  
22 monopile-supported offshore wind turbines using unscaled natural earthquake records”. *Soil  
23 Dynamics and Earthquake Engineering*, Vol 109, June, pp 154-172.
- 24 [9] Wind Africa: About the project 2018. Available at:  
25 <http://community.dur.ac.uk/wind.africa/about/>. [Accessed 23 Apr 2019].
- 26 [10] Wang, X., Ye, A., He, Z. and Shang, Y. 2015. “Quasi-Static Cyclic Testing of Elevated RC  
27 Pile-Cap Foundation for Bridge Structures”. *Journal of Bridge Engineering*, Vol 21, No 2,  
28 March, pp 1-16.
- 29 [11] Blanco, G., Ye, A., Wang, X. and Goicolea, J. 2018. “Parametric Pushover Analysis on  
30 Elevated RC Pile-cap Foundations for Bridges in Cohesionless Soils”. *Journal of Bridge  
31 Engineering*, Vol 24, No 1, November, pp 1-16.
- 32 [12] Albiker, J., Achmus, M., Frick, D. and Flindt, F. (2017). 1g model tests on the displacement  
33 accumulation of large-diameter piles under cyclic lateral loading. *Geotechnical Testing Journal*,  
34 Vol. 40, No. 2, pp. 173-184.
- 35 [13] Frick, D. and Achmus, M. (2019), Model tests on the behaviour of monopiles under general  
36 cyclic lateral loading, *2nd International Conference on Natural Hazards & Infrastructure*, 23-  
37 26 June, 2019, Chania, Greece.
- 38 [14] Bisoi, S and Haldar, S (2019), 3D Modeling of Long-Term Dynamic Behavior of Monopile-  
39 Supported Offshore Wind Turbine in Clay, *International Journal of Geomechanics*, Vol 19(7).
- 40 [15] Tziavos, I.N., Hemida, H., Metje, N. and Baniotopoulos, C. (2019), Non-linear finite element  
41 analysis of grouted connections for offshore monopile wind turbines, *Ocean Engineering* 171  
42 (2019), pp. 633–645.
- 43 [16] Chun-Bao, Y; Rui, W. and Jian-Min, Z. (2018), Seismic Analysis of Monopile Supported  
44 Offshore Wind Turbine, *International Conference on Geotechnical and Earthquake Engineering  
45 2018*, October 20–21, Chongqing, China.
- 46 [17] Reconan FEA v1.00, User’s Manual. 2010.
- 47 [18] Vu, A., Kobayashi, S., Matsumoto, T. and Nguyen, T. 2016. “Model load tests on battered pile  
48 foundations and finite-element analysis”. *International Journal of Physical Modelling in  
49 Geotechnics*, Vol 18, No 1, pp 33-52.
- 50 [19] Rajashree, S.S. and Sitharam, T.G. 2001. “Nonlinear Finite-Element Modeling of Batter Piles  
51 under Lateral Load”. *Journal of Geotechnical and Geoenvironmental engineering*, Vol 127, No  
52 7, pp 604-612.

- 1 [20] Prowell, I., Elgamal, A. and Lu, J. 2010. "Modelling the influence of soil structure interaction  
2 on the seismic response of a 5MW wind turbine. Scholars' Mine". Research 5.09a. San Diego,  
3 California.
- 4 [21] Guo, L., Uang, C., Elgamal, A., Prowell, I. and Zhang, S. 2011. "Pushover Analysis of a 53m  
5 High Wind Turbine Tower". *Journal of Computational and Theoretical Nanoscience*, Vol 4, No  
6 3, March, pp 656-662.
- 7 [22] Bathe, K.J. 1996. "Finite element procedures". Prentice-Hall, Upper Saddle River, New Jersey.
- 8 [23] Markou, G., Mourlas, C., Bark, H. and Papadrakakis, M. (2018), "Simplified HYMOD non-  
9 linear simulations of a full-scale multi-storey retrofitted RC structure that undergoes multiple  
10 cyclic excitations-An infill RC wall retrofitted study", *Engineering structures*, Vol 176,  
11 December, pp 829-916.
- 12 [24] Gravett, D.Z., Mourlas, C., Markou, G., and Papadrakakis, M. "Numerical Performance of a  
13 New Algorithm for Performing Modal Analysis of Full-Scale Reinforced Concrete Structures  
14 that are Discretized with the HYMOD Approach". *COMPADYN 2019, 7th ICCMSDEE*. 24-26  
15 June 2019. Crete. Greece.
- 16 [25] Mourlas, C., Papadrakakis, M. and Markou, G. (2017), "A Computationally Efficient Model  
17 for the Cyclic Behavior of Reinforced Concrete Structural Members", *Engineering Structures*,  
18 141, pp. 97–125.
- 19 [26] Kotsovos, M.D. and Pavlovic, M.N. (1995). "Structural concrete, finite element analysis for  
20 limit state design". Thomas Telford, London, UK.
- 21 [27] Markou, G. and Papadrakakis, M., "Accurate and Computationally Efficient 3D Finite Element  
22 Modeling of RC Structures", *Computers & Concrete*, 12 (4), pp. 443-498, 2013.
- 23 [28] Mourlas, C., Papadrakakis, M. and Markou, G. (2017), "A Computationally Efficient Model  
24 for the Cyclic Behavior of Reinforced Concrete Structural Members", *Engineering Structures*,  
25 141, pp. 97–125.
- 26 [29] Mourlas, C., Markou, G. and Papadrakakis, M. (2019), "Accurate and Computationally  
27 Efficient Nonlinear Static and Dynamic Analysis of Reinforced Concrete Structures  
28 Considering Damage Factors", *Engineering Structures*, 178 (2019), pp. 258–285.
- 29 [30] Mourlas, C., Markou, G., and Papadrakakis, M., "3D Detailed Modeling of Reinforced  
30 Concrete Frames Considering accumulated damage during static cyclic and dynamic analysis  
31 – new validation case studies", *COMPADYN 2019, 7th International Conference on  
32 Computational Methods in Structural Dynamics and Earthquake Engineering*, 24-26 June 2019,  
33 Crete, Greece.
- 34 [31] Markou, G. and Papadrakakis, M., "An Efficient Generations Method of Embedded  
35 Reinforcement in Hexahedral Elements for Reinforced Concrete Simulations", *Advances in  
36 Engineering Software ADES*, 45 (1), pp. 175-187, 2012.
- 37 [32] Markou, G. (2015), "Computational performance of an embedded reinforcement mesh  
38 generation method for large-scale RC simulations", *International Journal of Computational  
39 Methods*, 12(3), 1550019-1:48.
- 40 [33] Menegotto, M., and Pinto, P. E. (1973). "Method of analysis for cyclically loaded reinforced  
41 concrete plane frames including changes in geometry and non elastic behaviour of elements  
42 under combined normal force and bending." *Proc., IABSE Symp. on Resistance and Ultimate  
43 Deformability of Structures Acted on by Well Defined Repeated Loads*, Lisbon, Portugal, 15–  
44 22.
- 45 [34] Rashid, Y. 1968. "Analysis of prestressed concrete pressure vessels". *Nuclear Engineering and  
46 Design*, Vol 7, March, pp 334-344.
- 47 [35] Rama, S.J.K., Sivakumar, M.V.N., Garg, C., Walia, S. and Vasan, A. 2014. "A Review on  
48 Studies of Fracture Parameters of Self Compacting Concrete". *Advances in Structural  
49 Engineering*, December, pp 1705-1716.